Unifying large and small wave-generated ripples

Jon J. Williams, Paul S. Bell, and Peter D. Thorne
Proudman Oceanographic Laboratory, Liverpool, UK

Received 30 May 2004; revised 4 October 2004; accepted 19 November 2004; published 12 February 2005.

[1] Frequently, in field and laboratory studies of wave-generated bed forms on beds of sandy sediments, both large and small wave-generated ripples (LWRs and SWRs) are observed and in some situations may be superimposed upon one another. The present paper examines relationships between measured wave conditions and the geometry of LWRs and SWRs and shows that existing empirical equations used to predict the dimensions of SWRs perform badly for LWRs. To address this problem, relationships found between ripple geometry and the wave Reynolds number are used as the basis for new expressions for prediction of ripple height, wavelength, and steepness that improve the accuracy of existing approaches for both LWRs and SWRs. The present results indicate strongly that SWRs and LWRs are related and their superposition in certain conditions reflects the time lag between the response of the bed to changing hydrodynamic conditions. They must be considered therefore when estimating the total bed roughness in a range of practical engineering and numerical modeling applications.

Citation: Williams, J. J., P. S. Bell, and P. D. Thorne (2005), Unifying large and small wave-generated ripples, *J. Geophys. Res.*, *110*, C02008, doi:10.1029/2004JC002513.

1. Introduction

[2] Since pioneering experiments with oscillating trays of sediment in still water [*Bagnold*, 1946], many field and laboratory studies have examined the formation and geometry of wave-generated ripples on beds of sandy sediments. Most laboratory studies have examined regular wave flows and so-called equilibrium ripple conditions. Field studies have involved irregular flows and frequently temporal lags are observed between the wave-induced flow and ripple formation. As a result often nonequilibrium conditions pertain in the field and the geometry and migration rate of ripples and sediment transport depends on the previous flow and bed history as well as on the prevailing flow at the time of the observations. In laboratory and field studies the superposition of two or more bed form scales is often observed reflecting complex interplay between fluid flows and unconsolidated sediments acting over a range of different time and space scales. Advances in the understanding of processes leading to the formation of complex wave ripple patterns and improved methods of predicting ripple morphology are required in a number of important applications in numerical modeling of coastal seas (e.g., bed friction), sediment processes (e.g., mobilization, resuspension and transport), nearshore process studies (e.g., wave attenuation), coastal engineering (e.g., dredging, sediment ingress and infill), and Navy operations (e.g., mine burial prediction).

[3] In the case of wave-generated ripples it is possible to distinguish two types on the basis of scale and persistence. The first type encompasses the well-known relatively steep, small wave-generated ripples, SWRs, with heights, η, $O[5]$ cm and wavelengths, λ, $O[30]$ cm. These bed forms can be variously classified as orbital, suborbital, and anorbital [*Wiberg and Harris*, 1994] according to their geometry. Their formation from the rolling-grain stage and modifications thereafter generally occurs on the scale of minutes. The second type have been termed "large-scale oscillatory bed forms" with λ $O(1.0)$ m and η $O(0.01)$ m. These are generally low amplitude, gently sloping, long wavelength features, hereinafter referred to as large wave-generated ripples, LWRs, are usually associated with large wave orbital excursions. In certain conditions their surfaces are populated by smaller superimposed SWRs. Observations of LWRs are reported from flume experiments [e.g., *Carstens et al.*, 1969; *Southard et al.*, 1990; *Vincent et al.*, 2001; *Williams et al.*, 2000, 2004] and from the field [e.g., *Dingler and Inman*, 1976; *Osborne and Vincent*, 1993; *Gallagher et al.*, 1998; *Amos et al.*, 1988; *Boyd et al.*, 1988; *Drake and Cacchione*, 1989; *Hay and Wilson*, 1994; *Vincent et al.*, 1999; *Hume et al.*, 1999; *Li and Amos*, 1999; *Traykovski et al.*, 1999; *Doucette*, 2002a, 2002b; *Hanes et al.*, 2001; *Ardhuin et al.*, 2002]. In some situations, steeper LWRs may be present [e.g., *O'Donoghue and Clubb*, 2001]. These bed forms are not reported from the field and are normally associated with coarser sediments (i.e., median grain diameter, D_{50}, >0.3 mm) subjected to regular oscillatory flows in the laboratory. In reported tests SWRs are never present with these bed forms. While some authors make a distinction between SWRs and LWRs, the observation that both can coexist makes it is unclear if they are distinct bed forms produced by different mechanism or simply variants of the same bed feature.

[4] In most cases, the morphology of SWRs scales with the orbital diameter of waves close to the bed, d_o, and with

0148-0227/05/2004JC002513$09.00

D_{50}, and a number of empirical formulae relate η/D_{50} or λ/D_{50} to d_o/D_{50} and provide predictions of expected bed form dimensions. A large number are based on data from laboratory wave flume experiments in which the flow is regular, short period and low amplitude [e.g., *Inman*, 1957; *Dingler*, 1974; *Miller and Komar*, 1980; *Nielsen*, 1981; *Grant and Madsen*, 1982; *Vongvisessomjai*, 1984; *van Rijn*, 1989; *Wikramanayake*, 1993; *Wiberg and Harris*, 1994; *Mogridge et al.*, 1994; *Khelifa and Ouellet*, 2000; *Faraci and Foti*, 2002] and they generally perform well for a limited range of conditions. However, for regular and irregular flows with field-scale periods and orbital amplitudes, errors arise since hydrodynamic conditions may lie outside the calibration range of the formulae and the geometry of ripples may not often be in equilibrium with the flow conditions under which they are measured [e.g., *Kos'yan*, 1988; *Osborne and Vincent*, 1993; *Li et al.*, 1996; *Doucette*, 2002b]. For these reasons the formulae can seriously under- or overpredict ripple dimensions. This applies in particular to the LWRs discussed here.

[5] The paper attempts to answer four important questions related to wave-generated bed forms observed in the laboratory and the field.

[6] 1. What processes bring about the superposition of different bed form scales in a given hydrodynamic regime?

[7] 2. Why does measured wave-generated ripple geometry exhibit such a wide variance in essentially the same hydrodynamic conditions?

[8] 3. How does the superposition of bed forms influence the bed roughness?

[9] 4. From a practical standpoint, which are the best equations to use for predicting the geometry of SWRs and LWRs?

[10] To address these questions, data pertaining to SWRs and LWRs observed in large-scale laboratory experiments and in the field are examined and attempts are made to understand and predict observed morphology of SWRs and LWRs in terms of the observed hydrodynamic conditions producing these bed forms. Attention is given also to the classification of LWRs and to their relationship with SWRs observed at times to populate the surface of these larger bed forms. It will be shown that existing empirical approaches for the prediction of η, λ and ripple steepness, ϑ (i.e., η/λ), used for SWRs are not suitable for LWRs and thus alternative predictive tools for these bed forms are derived from the present data. A new "universal" predictive approach for any SWR or LWR is then developed through examination of the relationship between ripple geometry and the wave Reynolds number. With some exceptions, this technique spans a wide range of ripple forms and hydrodynamic conditions and makes it unnecessary to classify ripples before applying predictive formulae to estimate η, λ, and ϑ. Attention is then given to the four questions posed above using existing knowledge and results from the present study.

2. Data Sources and Instrumentation

[11] While there are a wide range of data sets related to wave-generated ripples available, few contain a complete record of ripple geometry, sediments and hydrodynamic parameters required for detailed analysis and even fewer encompass hydrodynamic regimes where SWRs and LWRs coexist. For this reason we are selective in our choice of data for the present study. The bulk of the present data set comes from measurements obtained in the large-scale Delta wave flume reported by *Williams et al.* [2000] (hereinafter referred to as "DFD" for the Delta flume data set; Tables A1 and A2) and from published measurements obtained in the field by *Hanes et al.* [2001]. Conveniently, both these data sets were obtained in a water depth, h, of approximately 4 m. The field data of *Hanes et al.* [2001] were obtained during three campaigns at the U.S. Army Corps of Engineers Field Research Facility at Duck, North Carolina. Using the *Hanes et al.* [2001] notation, these data sets are as follows: SIS95 (23 to 25 August 1995, 1.6 m < h < 6.8 m, 0.18 mm < D_{50} < 1.66 mm, 0.2 m < H_s < 0.9 m); SIS96 (29 October to 1 November 1996, 1.4 m < h < 7.0 m, 0.12 mm < D_{50} < 0.21 mm, 0.32 m < H_s < 1.2 m); and Sandyduck97 (11 September to 10 November 1997, 3.3 m < h < 5.2 m, D_{50} = 0.16 mm, 0.37 m < H_s < 2.3 m), where H_s is the significant wave height. During SIS95 and SIS96, data were obtained by deploying instruments from the research pier. During Sandyduck97, data were obtained from a fixed array if instruments in approximately 4 m water depth. For convenience the combined SIS95, SIS96 and the Sandyduck97 data sets are hereinafter referred to as "SDD" for the Sandyduck data set. In addition, field data related to SWRs from *Inman* [1957] and to mixed SWRs and LWRs from *Hume et al.* [1999] and *Doucette* [2002b] are also included in the present analysis. These data were obtained in water depths ranging from 1.4 m to 16.8 m in the case of *Inman* [1957] and 25 m in the case of *Hume et al.* [1999]. These additional data extend the range of hydrodynamic conditions and grain sizes considered here. The *Inman* [1957] and *Hume et al.* [1999] data are tabulated by *Williams et al.* [2004]. The *Doucette* [2002b] data are summarized in Table A3.

[12] Ripples were generated by waves in the Delta flume (h = 4.5 m] on beds of sand of depth 0.5 m which spanned the 5 m width of the flume and extended a length of 30 m. The median grain diameters, D_{50}, used in the two test sequences were 0.349 mm and 0.220 mm [see *Williams et al.*, 2004, Figure 1c]. Following *Williams et al.* [2003] measurements of the bed morphology were taken approximately 30 min after the start of a given wave run using an acoustic ripple profiler, ARP (available at http://www.marine-electronics.co.uk). In irregular waves tests showed that this time was sufficient for λ and η values to become approximately statistically stationary [*Williams et al.*, 2004]. The ARP, comprising of a 2MHz transducer mounted onto a motor [*Bell and Thorne*, 1997; *Bell et al.*, 1998], measured bed morphology along a line extended 4 m beneath the deployment frame along the streamwise axis of the flume at approximately 1 min intervals (Figure 1). Test were undertaken in irregular waves conforming to the JONSWAP spectrum with the significant wave height, H_s, in the range 0.20 m to 1.55 m and peak period, T_p, in the range 4 s to 6 s. Field measurements of wave-formed ripples comprising the SDD were obtained by acoustic means by *Hanes et al.* [2001] using a multiple acoustic transducer array [*Jette*, 1997; *Jette and Hanes*, 1998]. Further details of the instrumentation and data analysis used to obtain the SDD is given by *Hanes et al.* [2001]. Given that the measurements were obtained in the field it is not possible to assess

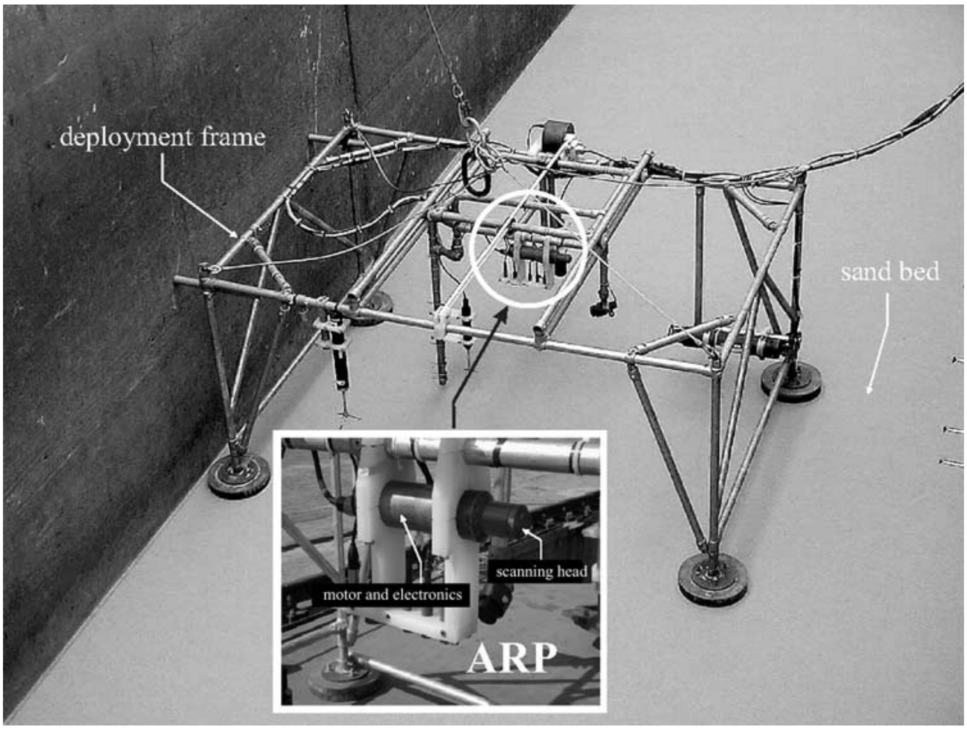

Figure 1. Deployment frame and instruments in the Delta flume (for details see *Williams et al.* [2004]). Inset shows the acoustic ripple profiler (ARP) used to measure bed ripples.

whether or not these ripples were fully in equilibrium with the prevailing hydrodynamic conditions.

[13] It is noted here that in the range of hydrodynamic conditions of the present experiments both two-dimensional (2-D) ripples, i.e., long-crested, parallel ripples with height and length constant over a large bed area and three-dimensional (3-D) ripples were observed. These different ripple morphologies are consistent with those reported in many laboratory and field settings [e.g., *Lofquist*, 1978; *Sato and Horikawa*, 1986; *Boyd et al.*, 1988; *Osborne and Vincent*, 1993; *Ribberink and Al-Salem*, 1994; *Traykovski et al.*, 1999; *Crawford and Hay*, 2001; *O'Donoghue and Clubb*, 2001; *Williams et al.*, 2003]. Since existing empirical formulae for prediction of ripple dimensions do not discriminate between 2-D, 3-D, or intermediate ripple forms and *Williams et al.* [2003] show that in cases of 3-D ripples in the Delta flume η and λ values are approximately spatially invariant we consider that η and λ values obtained from bed profiles by the methods outlined above are representative of the wider bed morphology. It is noted also that given the limited spatial extent of the present measurements it is thought possible that wave-generated bed forms at a scale presently undetected by the instruments may also exist.

3. Data Analysis

3.1. Delta Flume Data (DFD)

[14] Each ARP profile was edited to remove infrequent noise spikes attributable to local resuspension events and instrument noise. A digital filter was then used to separate the SWRs [cf. *Williams et al.*, 2004] from the LWRs present during some of the tests. Using zero down-crossing analysis software (available at http://www.maths.lth.se/matstat/wafo), spatially averaged values of λ and η for the SWRs and for LWRs were then obtained from each ARP profile. In cases where λ values were large (i.e., <1.5 bed form wavelengths present in a given ARP profile) a wavelet analysis (wavelet software was provided by C. Torrence and G. Compo, and is available at http://paos.colorado.edu/research/wavelets/) [*Torrence and Compo*, 1998] technique was used to determine values of λ and η [cf. *Metje et al.*, 2001]. The wave orbital diameter $d_o = H/\sinh(kh)$ where $H = H$ or H_s, k is the wave number $= 2\pi/L$, L is the wavelength of the surface gravity wave (i.e., $2\pi/k$) and the wave number, $k = \varphi/h$. Here φ is a dispersion parameter defined as $\varphi = \gamma^{1/2}(1 + 0.2\gamma)$ for $\gamma \leq 1$ and $\varphi = \gamma\,[1 + 0.2\exp(2 - 2\gamma)]$ for $\gamma > 1$ [*Soulsby*, 1997]. In the term $\gamma = \omega^2 h/g$, g is the acceleration due to gravity and $\omega = 2\pi/T$. The orbital amplitude A_o is defined as $d_o/2$. The peak semiorbital velocity close to the bed, u_w, was obtained from $u_w = \pi d_o/T_p$ and estimates of the wave-induced skin friction bed shear velocity, u_{*ws}, were obtained from $u_{*ws} = (0.5\,f_w u_w^2)^{0.5}$ where the wave friction factor, f_w, is defined in terms of the relative (grain) roughness, r, by *Soulsby* [1997] as $f_w = 1.39(0.5d_o/z_o)^{-0.52}$ and where the Nikuradse equivalent sand grain roughness is given by $z_0 = D_{50}/12$.

[15] The resulting hydrodynamic and sediment data were then used to calculate a number of useful dimensionless groupings. These included a wave "mobility number", ψ, defined as $\psi = \rho u_w^2/(\rho_s - \rho)gD_{50}$ [*Brebner*, 1980] where ρ_s is the sediment density (2650 kg/m^3) and ρ is the fluid density (1000 kg/m^3) used to characterize sediment dynamics: the Rouse number, $b = w_s/\kappa u_{*ws}$, where w_s is the grain settling velocity; the wave Shields number, $\theta_{\mathrm{wave}} = 0.5\,f_w\psi$; the orbital Reynolds number, $Re_{\mathrm{wave}} = A_o^2\omega/\upsilon$; the grain Rey-

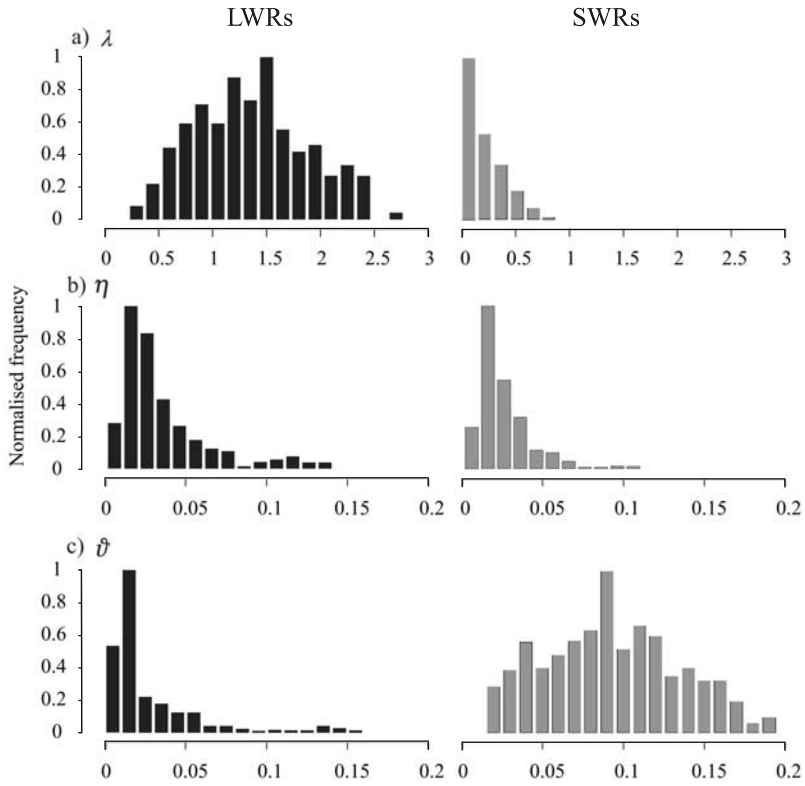

Figure 2. Histogram distributions showing the normalized frequency distributions for λ, η, and ϑ for LWRs and SWRs. Data from DFD, SDD, *Inman* [1957], *Hume et al.* [1999], and *Doucette* [2002b].

nolds number, $Re_{\mathrm{grain}} = A_o\ \omega D_{50}/\upsilon$. Here s is the specific gravity of the sediment (2.65). Tables summarizing hydrodynamic conditions associated with the DFD are given in Appendix A.

3.2. Sandyduck Data (SDD)

[16] Using measured bed profiles, *Hanes et al.* [2001] determined the shape and dimensions of bed forms using zero up-crossing and a least squares sinusoidal shape fitting techniques. These data analysis methods and the derivation of hydrodynamic parameters from measured wave conditions at the time of the ripple observations are described in detail by *Hanes et al.* [2001]. The published data set provides all the hydrodynamic variables necessary to estimate the various parameters outlined above.

4. Results and Discussion

[17] Histograms showing the normalized frequency distributions of λ, η and ϑ, for LWRs (data: DFD; SDD [*Hume et al.*, 1999; *Doucette*, 2002b] and SWRs (data: DFD suborbital ripples; SDD [*Inman*, 1957; *Doucette*, 2002b] are shown in Figure 2. Note that for convenience the term ripple data set (RDS) is now used to denote all SWR and LWR data from the DFD, SDD [*Inman*, 1957; *Hume et al.*, 1999; *Doucette*, 2002b]. Figure 2 shows that while η values for LWRs and SWRs are spread across approximately the same range of values, the distributions for λ and ϑ are quite different. There is a suggestion in this data therefore that SWRs and LWRs may be distinct morphological forms. This is considered further below in the light of other evidence.

[18] *Southard et al.* [1990] found the spacing of LWRs conformed approximately to that expected for orbital ripples (i.e., $0.65d_o$). In the case of the SDD we find that while $\overline{\lambda} = 0.79\overline{d}_o$, (the overbar indicates the mean value), the correlation between λ and d_o is not statistically significant with LWR spacing lying in the range $0.34\overline{d}_o < \lambda < 1.33\overline{d}_o$ (standard deviation = $0.25\overline{d}_o$). While LWR λ values from the DFD are found to be correlated with d_o ($R^2 = 0.65$), $\overline{\lambda} = 0.97\overline{d}_o$ and thus deviates significantly from the value given by *Southard et al.* [1990]. No statistically significant correlation is found between η values for the LWRs and d_o. Given that λ and η are poorly correlated with d_o or u_{*ws} it appears that the geometry of the present LWRs cannot be explained simply in terms of the hydrodynamic forcing and thus account must also be taken of the sediment properties.

[19] To examine differences between SWRs and LWRs further it is helpful to examine the data sets using relationships between single parameters and dimensionless groupings of hydrodynamic and sediment properties. Principle amongst these are: η, λ, ϑ, λ/D_{50}, λ/D_{50}, η/D_{50}, d_o/D_{50}, d_o/η, η/A_0, λ/A_0, ϑ/A_0, Ψ, θ_{wave}, Re_{wave} and Re_{grain} and b. Relationships between these various parameters form the basis of many empirical predictive formulae for λ and η of wave-generated ripples and thus require examination using the present data set. As a starting point, Figure 3 shows η, λ and ϑ values plotted as a function of ψ, θ_{wave}, Re_{wave} and Re_{grain} for the RDS. Here clusters of data values can be identified with LWR values apparently separately from

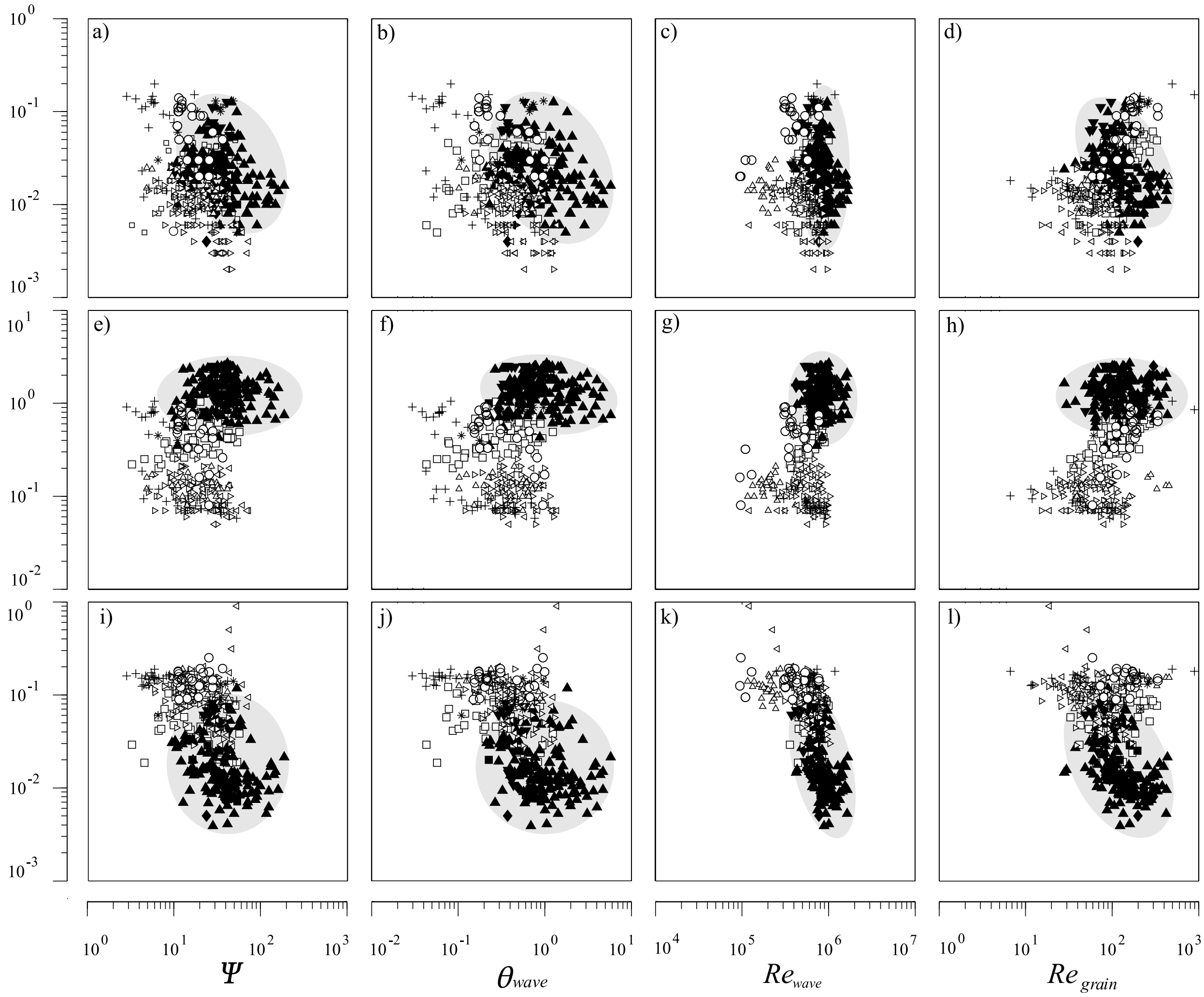

Figure 3. The η, λ, and ϑ as a function of ψ, θ_{wave}, Re_{wave}, and Re_{grain} for the RDS. Symbols for LWRs are as follows: solid diamond, Delta flume (D_{50} = 0.349 mm); solid square, Delta flume (D_{50} = 0.220 mm); solid triangle pointing down, SIS96 [*Hanes et al.*, 2001]; solid triangle pointing up, Sandyduck97 [*Hanes et al.*, 2001]. Symbols for SWRs are as follows: open square, Delta flume suborbital (all tests); open triangle pointing up, SIS95 [*Hanes et al.*, 2001]; open triangle pointing left, SIS96 [*Hanes et al.*, 2001]; open triangle pointing right, Sandyduck97 [*Hanes et al.*, 2001]; plus sign, *Inman* [1957]; asterisk, *Hume et al.* [1999]; and solid circle, *Doucette* [2002b]. Note that LWRs are indicated by the shaded gray areas.

SWR values in most of the plots. These LWR clusters are highlighted by the gray shaded areas on each subplot. There is considerable scatter in the data with no discernable trends. Similar comments apply to the results presented in Figure 4 which shows η/D_{50}, λ/D_{50}, and ϑ/D_{50} as a function ψ, θ_{wave}, Re_{wave} and Re_{grain}. Here, an attempt to normalize the data sets using a fundamental sediment parameter has failed to provide any statistically significant relationships between ripple geometry and hydrodynamic parameters.

[20] Following previously published work the RDS is now examined using some common dimensionless groupings frequently used in empirical expressions for predicting ripple dimensions. Using D_{50} as the factor to create dimensionless groupings, Figures 5a, 5b, and 5c show λ/D_{50}, η/D_{50} and ϑ as a function of d_o/D_{50}, respectively. Also included in Figure 5 are empirical curves fitted to the water tunnel data of *Mogridge and Kamphuis* [1972] by *Mogridge et al.* [1994], hereinafter referred to as MDW curves. Figure 5b also shows lines proposed by *Miller and Komar* [1980] and *Southard et al.* [1990] for orbital ($\lambda = 0.65d_o$) and anorbital ripples ($\lambda \approx 400D_{50} - 600D_{50}$). While there is a considerable scatter of data points, two clear groupings are again evident in each plot: one for SWRs; and a second for LWRs (identified by the gray shaded areas). Using a combination of D_{50} and d_o as the factors to create dimensionless groupings, Figures 6a and 6b show λ/D_{50} and ϑ values plotted as a function of d_o/η, respectively, and include MDW curves. In addition, Figure 6c uses A_o as the factor to create dimensionless groupings and shows η/A_0 as a function of λ/A_0 and includes the MDW curve. While the scatter of data points is reduced on this plot, prediction of ripples requires knowledge a priori of either λ or η and thus this relationship remains of limited usefulness.

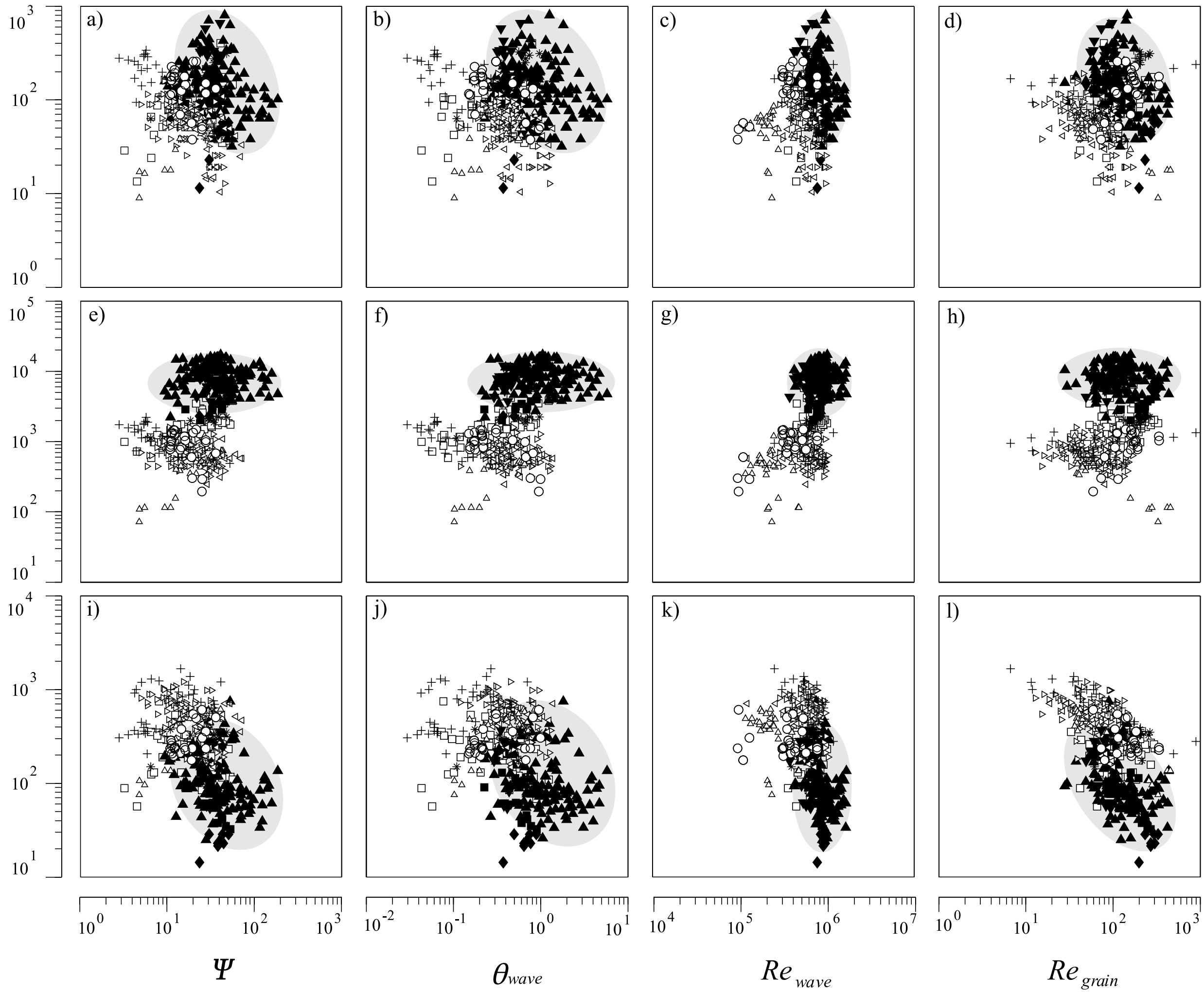

Figure 4. The η/D_{50}, λ/D_{50}, and ϑ/D_{50} as a function of ψ, θ_{wave}, Re_{wave} and Re_{grain} for the RDS. Symbols for the LWRs are as follows: solid diamond, Delta flume (D_{50} = 0.349 mm); solid square, Delta flume (D_{50} = 0.220 mm); solid triangle pointing down, SIS96 [*Hanes et al.*, 2001]; solid triangle pointing up, Sandyduck97 [*Hanes et al.*, 2001]; Symbols for the SWRs are as follows: open square, Delta flume suborbital (all tests); open triangle pointing up, SIS95 [*Hanes et al.*, 2001]; open triangle pointing left, SIS96 [*Hanes et al.*, 2001]; open triangle pointing right, Sandyduck97 [*Hanes et al.*, 2001]; plus sign, *Inman* [1957]; asterisk, *Hume et al.* [1999]; and solid circle, *Doucette* [2002b]; Note that LWRs are indicated by the shaded gray areas.

[21] The functional relationship between η/A_0 or λ/A_0 and Ψ provide the basis of many empirical formulae for the prediction of ripple geometry [*Soulsby*, 1997]. Thus in an attempt to find a statistically significant relationships between ripple geometry and hydrodynamics for the RDS, Figures 7a and 7b show η/A_0 and λ/A_0 as a function of Ψ, respectively, together with a number of curves predicted by empirical expressions. These include MDW curves and empirical predictions from the *Nielsen* [1981], (hereinafter referred to as N-81), *Grant and Madsen* [1982] (hereinafter referred to as GM-82) and *Van Rijn* [1989] (hereinafter referred to as VR-89) equations. For clarity these are shown in the top panels of Figures 7a and 7b together with gray shading indicating the location of the SWR and LWR data clusters. The expressions for these various curves are given in Appendix B. It is evident that in common with the previous plots there is considerable scatter in the LWR and SWR data sets. In the case of η/A_0, Figure 7a shows that the GM-82 curve gives the best fit to the SWR data. However, while N-81, GM-82 and VR-89 equations pass through the LWR and SWR data clusters, they fail to predict LWRs at Ψ values beyond around 150. The GM-82 and N-81(field) curves seriously underpredict η/A_0 values across all Ψ values. The MDW curve performs much better in this respect and passes approximately through the center of the LWR data cluster and extends to high Ψ values. None of these equations performs well against the LWR data set for λ/A_0, and each predicts rather different λ/A_0 values for the SWRs. In this case the N-81(field) curve gives the best fit to the data. The fitted curves derived for the RDS are shown in the bottom panel of Figures 7a and 7b together with the data. These various curves take the form

$$\frac{\eta_l}{A_o} = \exp\left[-0.2043\ \ln(\Psi)^2 + 1.279\ \ln(\Psi) - 4.808\right], \qquad (1)$$

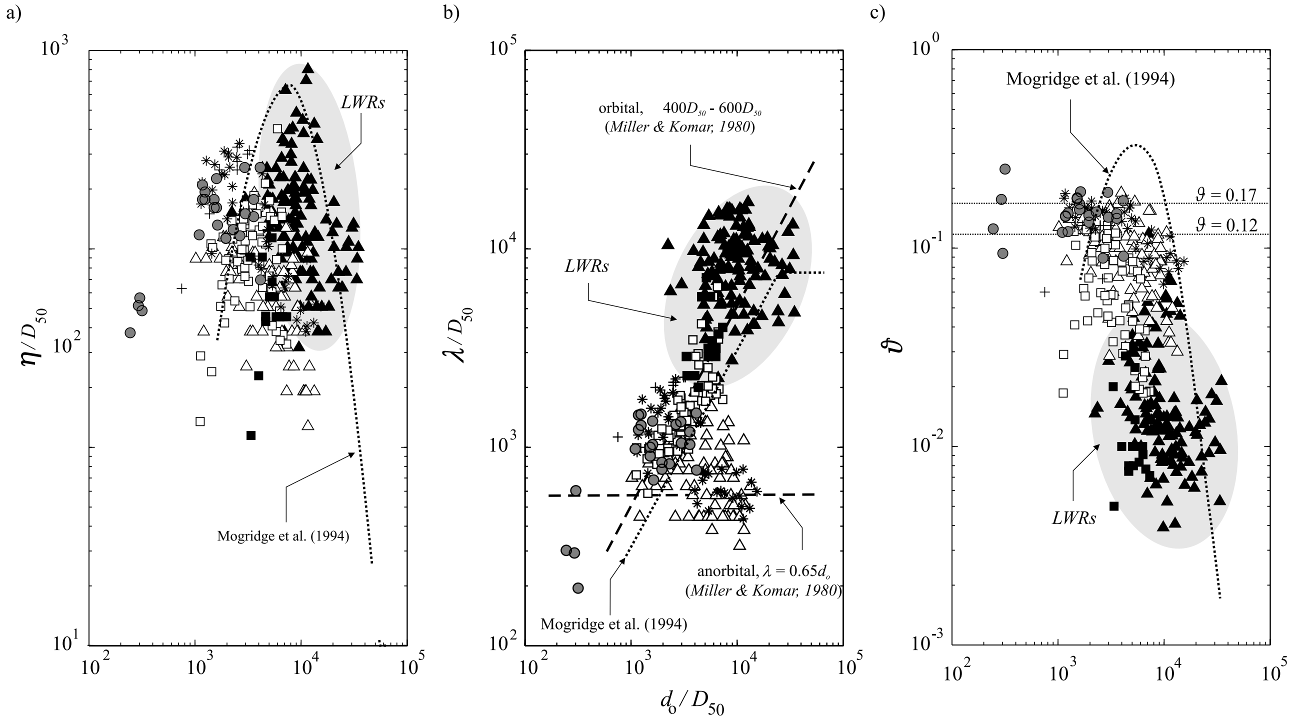

Figure 5. (a) Normalized ripple height, η/D_{50}, as a function of normalized wave orbital diameter, d_0/D_{50}; (b) normalized ripple wavelength, λ/D_{50}, as a function of d_0/D_{50}; and (c) ripple steepness, ϑ, as a function of d_0/D_{50}. Symbols for LWRs are as follows: solid square, Delta flume; solid triangle, SIS96 and Sandyduck97 [*Hanes et al.*, 2001]; Symbols for SWRs are as follows: open square, Delta flume; open triangle, SIS95, SIS96, and Sandyduck97 [*Hanes et al.*, 2001]; plus sign, *Inman* [1957]; asterisk, *Hume et al.* [1999]; and solid circle, *Doucette* [2002b]. Note that LWRs are indicated by the shaded gray areas.

(R^2 = 0.40) and

$$\frac{\lambda_l}{A_o} = \exp\left[-0.2007\ \ln(\Psi)^2 + 1.467\ \ln(\Psi) - 1.718\right], \quad (2)$$

(R^2 = 0.51) for LWRs; and

$$\frac{\eta_s}{A_o} = \exp\left[-0.0282\ \ln(\Psi)^2 - 1.418\ \ln(\Psi) + 1.249\right], \quad (3)$$

(R^2 = 0.67) and

$$\frac{\lambda_s}{A_o} = \exp\left[0.0542\ \ln(\Psi)^2 - 1.307\ \ln(\Psi) + 2.843\right], \quad (4)$$

(R^2 = 0.65) for the SWRs, where the subscripts l and s refer to LWRs and SWRs, respectively. While not having a high degree of statistical significance, these equations nevertheless have a capacity to predict with greater precision η and λ values for the present data set than the published equations defined in Appendix B.

[22] Following *Wiberg and Harris* [1994], Figures 8a and 8b show b as a function of d_o/η and d_o/λ, respectively, for the RDS. Figure 8a shows that the bulk of the RDS is relatively closely grouped and spans the range of d_o/η values distinguishing suborbital and anorbital ripples [cf. *Wiberg and Harris*, 1994]. Generally, LWRs are associated with lower b values than SWRs. Here we combine LWR and SWR data sets to obtain the best fit line for prediction of η for SWRs and LWRs in the form

$$\frac{d_o}{\eta_{s,m}} = \exp\left[0.0461\ \ln(b)^2 - 0.6382\ \ln(b) + 2.729\right], \quad (5)$$

(R^2 = 0.32).

[23] Figure 8a shows also that SWRs and LWRs can exist at the same d_o/η value and thus the usefulness of d_o/η and/or b as a mean of discriminating between orbital, suborbital and anorbital ripples for situations where SWRs and LWRs coexist is clearly problematic. It is evident also that the *Doucette* [2002b] data lies well outside the range of the rest of the RDS. It is considered that this arises since the ripples comprising this data set were formed in an environment markedly different from that for the other ripples. In Figure 8b, SWR and LWR d_o/λ values separate into two data clusters, each described by the curves

$$\frac{d_o}{\lambda_l} = \exp\left[-0.0998\ \ln(b)^2 - 0.3006\ \ln(b) + 0.8322\right], \quad (6)$$

(R^2 = 0.40) for LWRs; and

$$\frac{d_o}{\lambda_s} = \exp\left[0.0952\ \ln(b)^2 - 0.6686\ \ln(b) + 1.9269\right], \quad (7)$$

(R^2 = 0.42) for the SWRs. Again we find that LWRs are associated with lower b values than SWRs. Potentially,

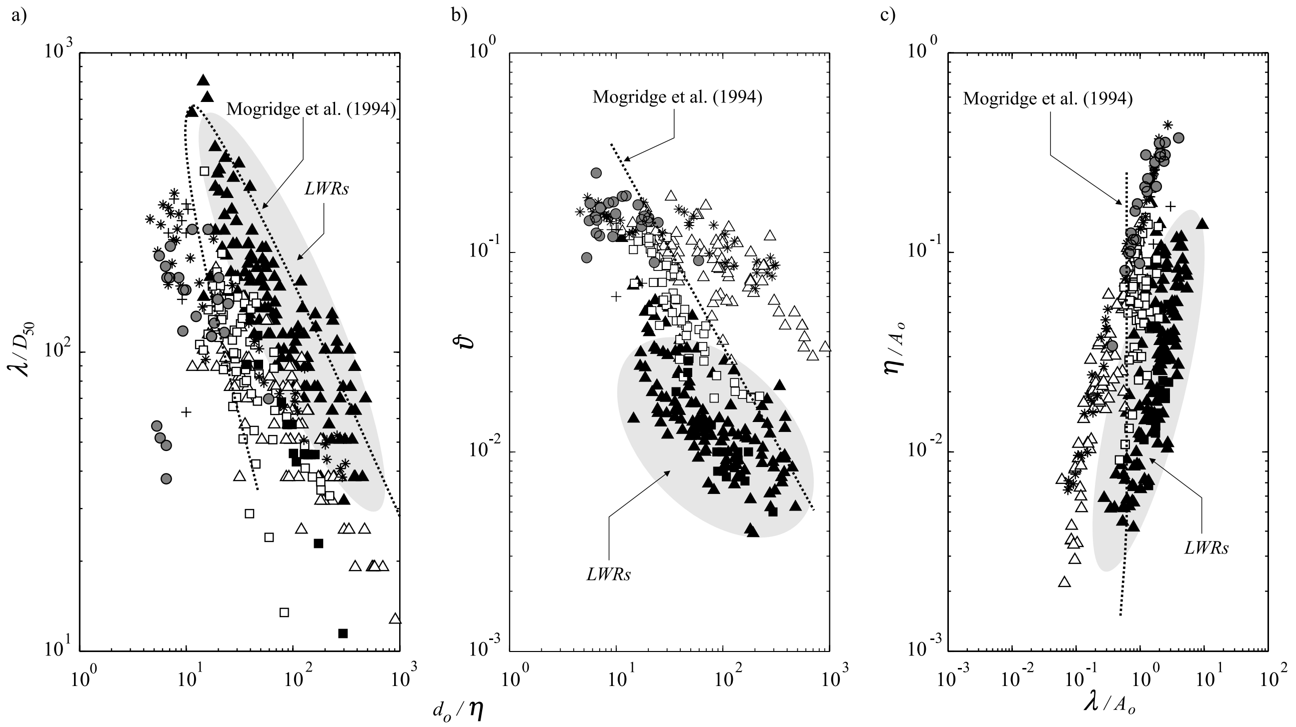

Figure 6. (a) Normalized ripple wavelength λ/D_{50} and (b) ripple steepness, ϑ, as a function of d_0/η, and (c) normalized ripple height, η/A_0, as a function of normalized ripple wavelength λ/A_0. Symbols for LWRs are as follows: solid square, Delta flume; solid triangle, SIS96 and Sandyduck97 [*Hanes et al.*, 2001]; Symbols for SWRs are as follows: open square, Delta flume; open triangle, SIS95, SIS96, and Sandyduck97 [*Hanes et al.*, 2001]; plus sign, *Inman* [1957]; asterisk, *Hume et al.* [1999]; and solid circle, *Doucette* [2002b]. Note that LWRs are indicated by the shaded gray areas.

equations (5)–(7) provide another means of predicting the dimensions of both SWRs and LWRs based upon readily obtainable hydrodynamic and sediment parameters. Each has a capacity to give predictions closer to the present data set than existing empirical equations. However, the data scatter is still relatively wide and errors in predicted ripples dimensions are likely to be correspondingly large. It is necessary also to make a distinction between SWRs and LWRs in order to apply these expressions correctly and a suitable method by which to do this remains unclear.

[24] Together Figures 5 to 8 show that for the RDS, relationships between parameters expressing ripple geometry, sediment properties and hydrodynamic conditions exhibit wide scatter. Thus in order to meet a desired requirement for accurate prediction of ripple geometry alternative approaches must be sought. Exploring further other potentially useful relationships between ripple dimensions and hydrodynamic conditions Figure 9 shows η/A_0, λ/A_0 and ϑ/A_0 as a function of θ_{wave}, Re_{wave}, and Re_{grain}. While there is no statistically significant relationship in the plots using the θ_{wave} and Re_{grain} parameters, graphs showing η/A_0, λ/A_0 and ϑ/A_0 as a function of Re_{wave} show how the RDS collapses to produces a narrower data cluster and provide an opportunity therefore to derive more precise expressions for the prediction of η and λ values for both LWRs and SWRs. For clarity, these plots are shown in enlarged form in Figure 10.

[25] Figure 10a shows η/A_0 as a function Re_{wave}. With the exception of the SWR data from *Hanes et al.* [2001], (i.e., SWRs measured during SIS95 and SIS96) the remaining 83% of the RDS (including SWRs from Sandyduck97) conform approximately to a curve in the form

$$\eta_{l,\mathrm{sub},s}/A_o = \exp^{[-1.037\ \ln(Re_{\mathrm{wave}})+10.30]}, \tag{8}$$

(R^2 = 0.38). Here the subscript "sub" is used to distinguish suborbital ripples. Forming their own distinct data subset, the relationship between η/A_0 and Re_{wave} for the SWRs measured during SIS95 and SIS96 by *Hanes et al.* [2001] exhibits rather different behavior from the other data and for this reason we have excluded these data from the analysis. In attempting here to explain why these data differ from the other data in the RDS it is first assumed that the method used to deploy the instruments did not affect the ripple formation processes. Since the bulk of the data were obtained in shoaling waves, and in some case shoreward migration of SWRs and LWRs was reported by *Hanes et al.* [2001], it is thought that a possible contributing factor concerns wave asymmetry which may have modified SWR ripple formation processes. Further, data were obtained at different shore-normal locations where differences in grain size between sites were large (i.e., 0.12 mm to 1.66 mm) and where bed slope may have been variable owing to the presence of bar systems. However, without further data it is not possible to explain fully these differences.

[26] In Figure 10b, λ/A_0 is plotted as a function Re_{wave} and shows three distinct clusters of data: the SWRs;

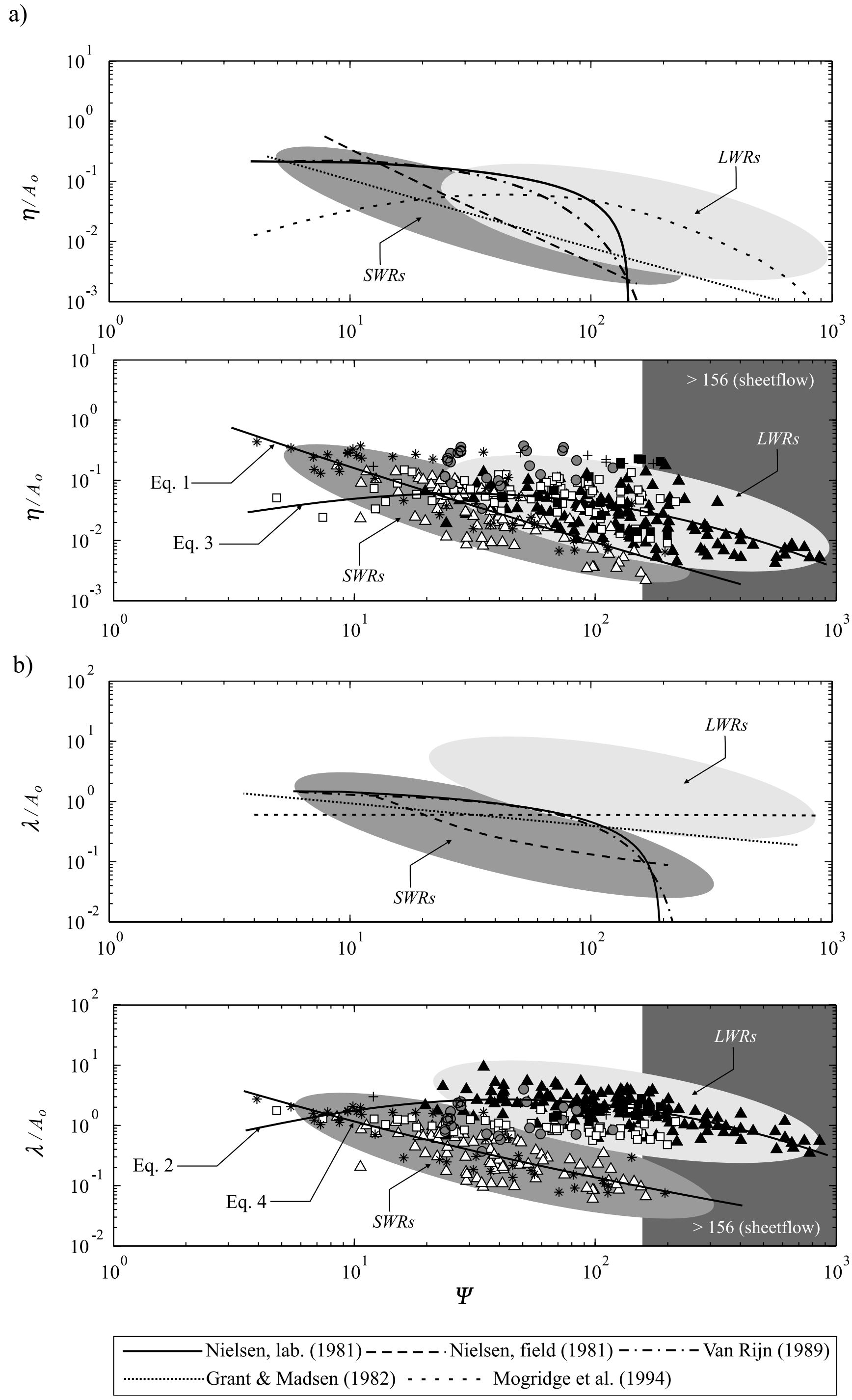

Figure 7. (a) Normalized ripple height, λ/A_0, as a function of the mobility number, ψ, and (b) normalized ripple wavelength, λ/A_0, as a function of ψ. Symbols for LWRs are as follows: solid square, Delta flume; solid triangle, SIS96 and Sandyduck97 [*Hanes et al.*, 2001]; Symbols for SWRs are as follows: open square, Delta flume; open triangle, SIS95, SIS96, and Sandyduck97 [*Hanes et al.*, 2001]; plus sign, *Inman* [1957]; asterisk, *Hume et al.* [1999]; and solid circle, *Doucette* [2002b]. Note that LWRs are indicated by the shaded gray areas.

suborbital ripples from the DFD; and LWRs. Again we exclude SWR data from SIS95 and SIS96 from the RDS the best fit relationships for LWRs, suborbital ripples and SWRs take the form

$$\lambda_l/A_o = \exp^{[-0.938 \ln(Re_{\text{wave}})+13.28]}, \quad (9)$$

$(R^2 = 0.57)$

$$\lambda_{\text{sub}}/A_o = \exp^{[-0.290 \ln(Re_{\text{wave}})+3.78]}, \quad (10)$$

$(R^2 = 0.15)$

$$\lambda_s/A_o = \exp^{[-1.036 \ln(Re_{\text{wave}})+12.28]}, \quad (11)$$

$(R^2 = 0.43)$.

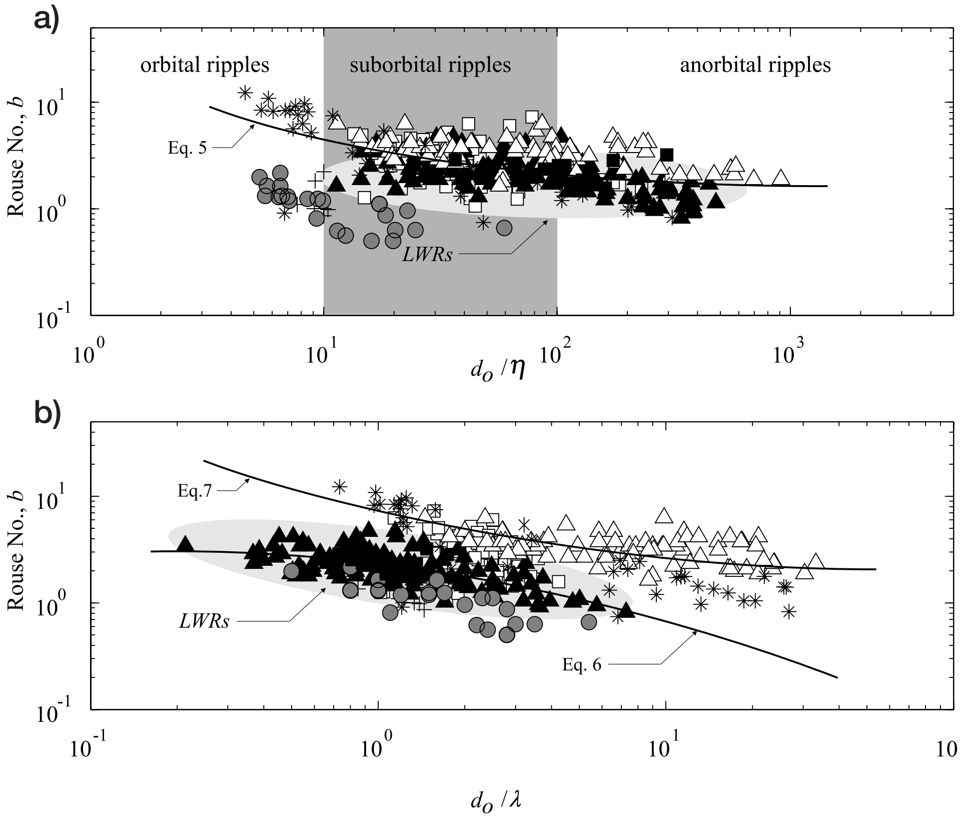

Figure 8. Rouse number (b) as a function of (a) d_0/η showing the subdivision between orbital, suborbital, and anorbital ripples proposed by *Wiberg and Harris* [1994] and (b) d_0/λ. Symbols for LWRs are as follows: solid square, Delta flume; solid triangle, SIS96 and Sandyduck97 [*Hanes et al.*, 2001]; Symbols for SWRs are as follows: open square, Delta flume; open triangle, SIS95, SIS96, and Sandyduck97 [*Hanes et al.*, 2001]; plus sign, *Inman* [1957]; asterisk, *Hume et al.* [1999]; and solid circle, *Doucette* [2002b]. Note that LWRs are indicated by the shaded gray areas.

[27] It is noted that the correlation between the variables is still only weak and thus an ability to improve the accuracy of bed form dimension predictions by this approach remains elusive. However, a statistically significant fit to ϑ/A_0 versus Re_{wave} is shown in Figure 10c. Excluding *SWR* data from SIS95 and SIS96 from the RDS the curve takes the form

$$\vartheta_{l,\mathrm{sub},s}/A_o = \exp^{[-1.89\ \ln(Re_{\mathrm{wave}})+22.32]}, \qquad (12)$$

($R^2 = 0.67$)
Equation (12) offers therefore potentially a new expression for prediction of ripple steepness for a wide range of grain sizes and hydrodynamic conditions.

[28] Attention is now given to a discussion based upon a synthesis of the results and observations given above in an attempt to answer the four questions posed in the introduction. The first of these concerns the processes bringing about the superposition of different bed form scales in a given hydrodynamic regime. Here two possibilities are suggested by the present data: firstly SWRs and LWRs are formed by different processes at work in the same hydrodynamic regime and that some threshold exists below which LWRs cannot be generated; and secondly, ripples are formed by the same processes, but long, low amplitude ones may persist through time as new smaller ripples are formed in response to changing hydrodynamic conditions. To address this question we must first examine the possible mechanisms responsible for generating SWRs and LWRs and see if there are any similarities. On the basis of established theory it is assumed that the formation, orientation and migration of SWRs is related to the local wave-induced flow field as described by e.g., *Nielsen* [1992] and *Soulsby* [1997]. Here attention is focused on possible mechanisms leading to the formation of the less well-studied LWRs. If these can coexist or even enhance the mechanisms responsible for formation of SWRs, it might explain how the two ripple types come to be superimposed in certain condition.

[29] It is first noted that the η and ϑ values reported here for LWRs are generally lower than those reported from previous observations [e.g., *Osborne and Vincent*, 1993; *Gallagher et al.*, 1998; *Thornton et al.*, 1998]. This raises the question of whether the oscillatory flow adjacent to the present LWRs actually separates to create the shear stress distribution necessary for normal wave-related ripple formation processes. Using the measured bed form shapes and wave forcing, *Hanes et al.* [2001] used the DUNE 2D model [*Tjerry*, 1995; *Andersen*, 1999] to simulate the boundary layer above their measured bed forms. In cases of LWR alone, results from the model showed only weak flow separation and turbulence generation and thus suggested strongly that processes forming LWRs are unrelated

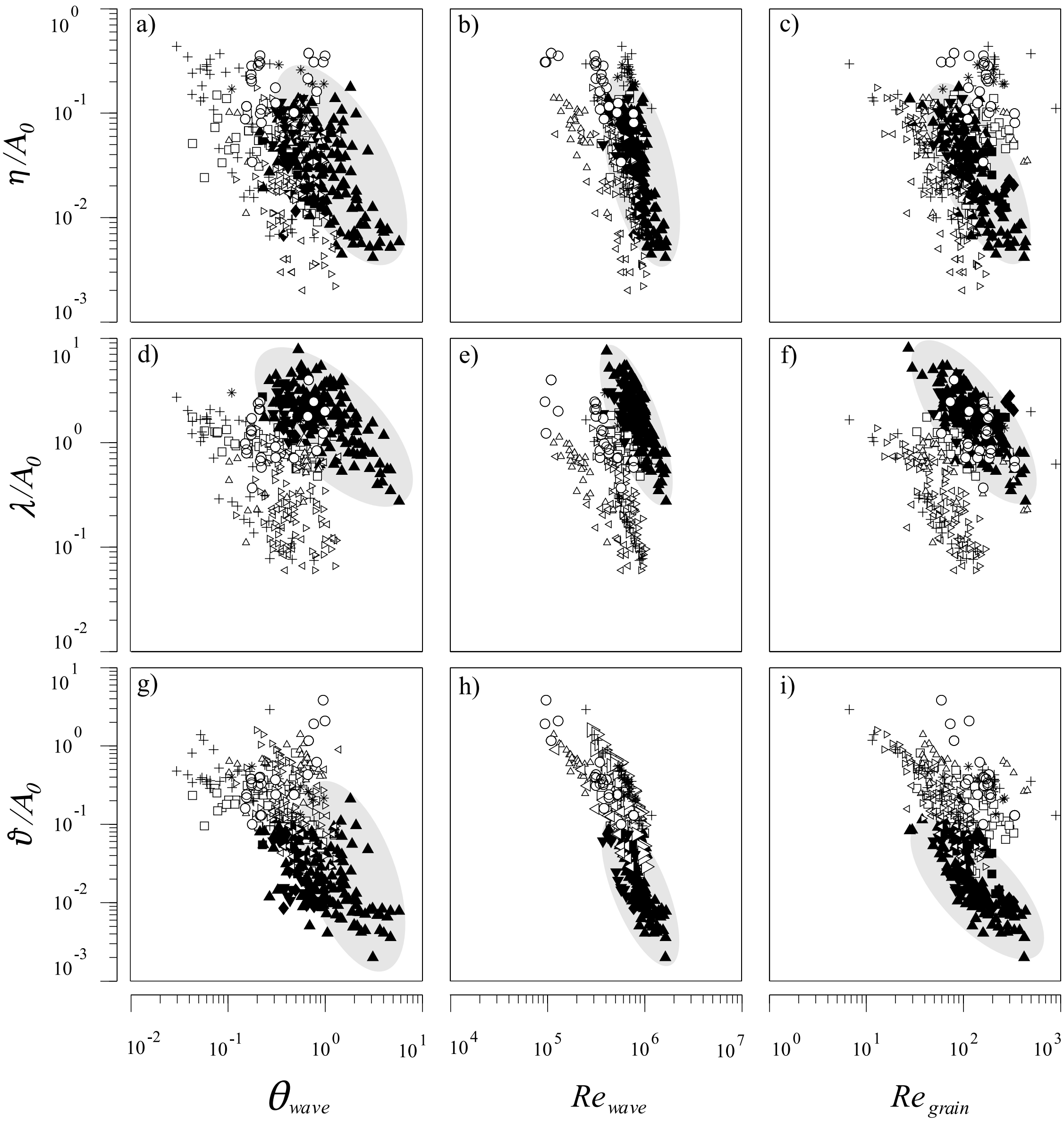

Figure 9. The η/A_0, λ/A_0, and ϑ/A_0, as a function of ψ, θ_{wave}, Re_{wave} and Re_{grain} for the RDS. Symbols for LWRs are as follows: solid diamond, Delta flume (D_{50} = 0.349 mm); solid square, Delta flume (D_{50} = 0.220 mm); solid triangle pointing down, SIS96 [*Hanes et al.*, 2001]; solid triangle pointing up, Sandyduck97 [*Hanes et al.*, 2001]. Symbols for SWRs are as follows: open square, Delta flume suborbital (all tests); open triangle pointing up, SIS95 [*Hanes et al.*, 2001]; open triangle pointing left, SIS96 [*Hanes et al.*, 2001]; open triangle pointing right, Sandyduck97 [*Hanes et al.*, 2001]; plus sign, *Inman* [1957]; asterisk, *Hume et al.* [1999]; and solid circle, *Doucette* [2002b].

to those for typical SWRs. In a similar approach used here results from a 1DV boundary layer model [*O'Connor et al.*, 1994] gave essentially the same results showing that flow separation and associated turbulence generation did not occur above LWRs and was most intense for bed forms with dimensions similar to SWRs. This evidence suggests strongly that the mechanisms leading to formation of LWRs are unrelated to those forming SWRs and alternatives must be examined.

[30] As flat bed conditions would normally be expected the simple fact that bed forms are observed at all in washout conditions when Ψ > 156 [*Nielsen*, 1992] is unexpected. It is noted also that LWRs persist for periods of hours in high wave conditions and show little tendency to diminish in height. A possible mechanism contributing to the formation and maintenance of LWRs at these high wave mobility numbers originally put forward by *Wiberg and Harris* [1994] concerns the periodic deposition and resuspension of suspended sediment around the times of flow reversal and flow maxima, respectively. This mechanism is suggested to result in the generation of low amplitude ripples with relatively long wavelengths scaling approximately with A_o. This is supported by evidence from the present data set which shows that that λ values

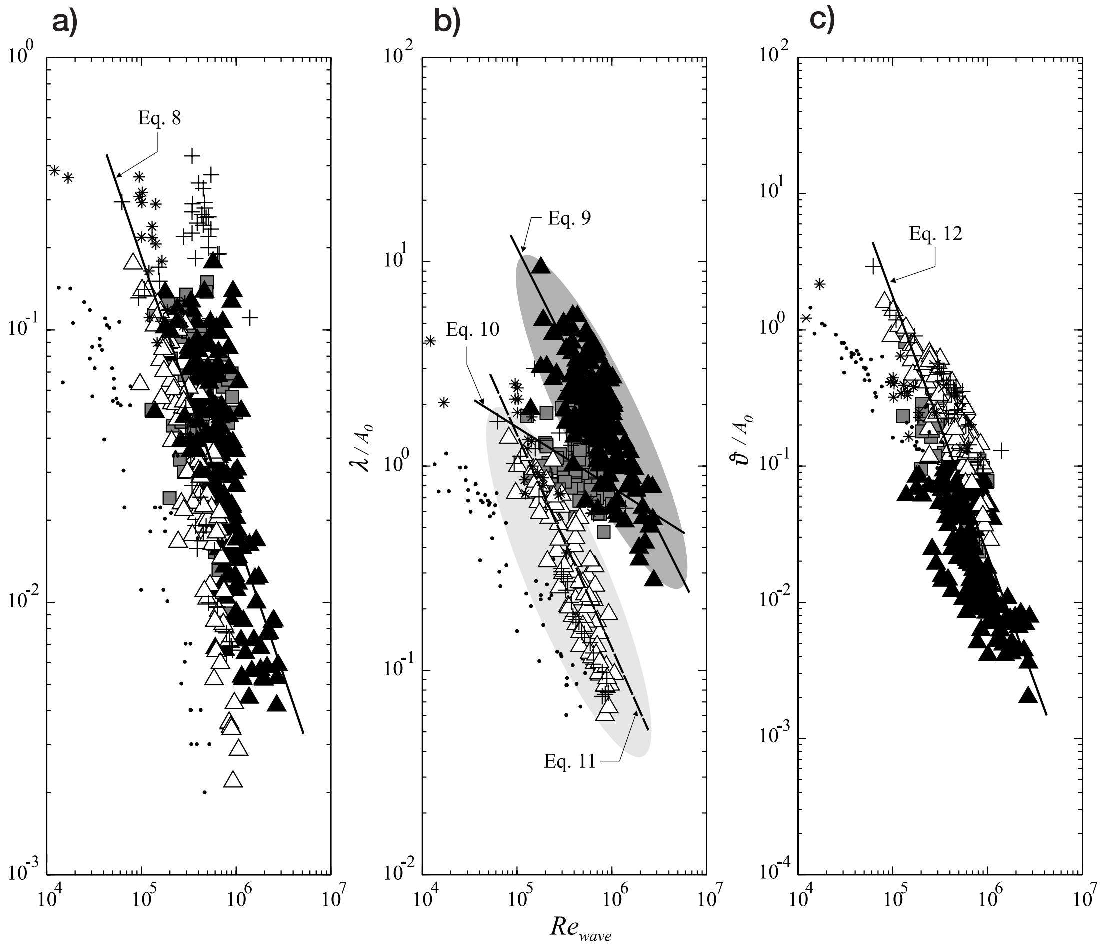

Figure 10. The η/A_0, λ/A_0, and ϑ/A_0, as a function of $\mathrm{Re}_{\mathrm{wave}}$ for the RDS. Symbols for LWRs are as follows: solid triangle, Delta flume (D_{50} = 0.349 mm), Delta flume (D_{50} = 0.220 mm), and SIS96 and Sandyduck97 [*Hanes et al.*, 2001]. Symbols for SWRs are as follows: solid square, Delta flume suborbital (all tests); SIS95 and SIS96 [*Hanes et al.*, 2001]; open triangle pointing up, Sandyduck97 [*Hanes et al.*, 2001]; plus sign, *Inman* [1957]; asterisk, *Hume et al.* [1999]; and solid circle, *Doucette* [2002b].

for LWRs in all lie within a factor of approximately 2 of d_o. Until the recent development of bed form measurement techniques in the field, it was thought that the conditions necessary to support the development of such bed forms could only exist in the laboratory since the vertical diffusion and advection of suspended sediment resulting from weak currents would act to suppress such bed form development. The DFD and SDD show clearly the persistence of LWRs for $\Psi > 156$ and thus for at least part of the wave cycle a significant amount of sediment in suspension would be expected in a high-concentration near-bed layer (Figure 7). This is supported by evidence of high suspended sediment concentrations measured in the Delta flume by acoustic means [*Williams et al.*, 2003] in a region extending 1 cm above the bed. Thus the conditions necessary to support the generation mechanism for LWRs suggested by *Wiberg and Harris* [1994] are observed to exist.

[31] A further and related mechanism to be implicated in the formation of LWRs through enhancement of the near bed sediment transport concerns the residual flows associated with waves. Principal among these is the steady wave streaming (or mass transport) effect [*Longuet-Higgins*, 1953] which refers to the wave-induced residual driven by vertical wave velocities occurring in the wave direction at the edge of the wave boundary layer above a plane bed for low waves. Given the uncertainties associated with sediment thresholds, settling velocity etc. it is considered here to be unproductive to use complex models of the wave boundary layer (wbl) to assess the possible role of wave streaming in ripple formation processes. Here we adopt a simple approach where the Eulerian drift velocity (or wave-induced streaming) for sinusoidal waves at the upper level of the wave boundary layer, U_∞ is given approximately by the expression

$$U_\infty = \frac{3k}{4\omega}\left(\frac{gkA_o}{\omega\cosh(kh)}\right)^2. \tag{13}$$

While in the present case it is necessary to also add an additional term to equation (13) to account for wave asymmetry, [e.g., *Fredsøe*, 1984], here for simplicity we assume wave asymmetry adds a further 10% to U_∞ values predicted by equation (13).

[32] In order to assess the ability of these wave-induced flows to move sediment it is necessary to estimate the resulting bed shear stress due to U_∞ and the threshold bed shear stress for the sediment. Here we assume a log profile in the thin wave boundary layer so that the skin friction bed shear stress related to wave streaming, τ_{ws}, is given by

$$\tau_{ws} = \rho\left(\frac{\kappa U_\infty}{\ln(\delta_w/z_o)}\right)^2, \tag{14}$$

where κ is the Karman constant = 0.4 and δ_w is the thickness of the wbl (i.e., $\sqrt{2\nu/\omega}$). The threshold skin friction shear stress values, $\tau_{\rm crit}$, were calculated using

$$\tau_{\rm crit} = \theta_{\rm crit} g(\rho_s - \rho)D_{50}, \tag{15}$$

where the critical Shields parameter is defined as

$$\theta_{\rm crit} = \frac{0.3}{1+1.2D_*} + 0.055\left[1 - \exp\left(-0.020D_*\right)\right]. \tag{16}$$

Soulsby [1997], and the dimensionless grain parameter is defined as

$$D_* = \left(g(s-1)/\nu^2\right)^{1/3} D_{50}.$$

[33] Results from a simulation using equation (13) are presented in Figure 11 which shows U_∞ as a function of A_o for the range 0.5 m < A_o < 1.5 m (typical of the RDS) in the top panels of Figures 11a–11c and τ_{ws} as a function of U_∞ in the bottom panels of Figures 11a–11c for D_{50} = 0.157 mm, 0.220 mm and 0.349 mm, T = 4 s, 6 s, 8 s and 10 s, in water depths of 4.5 m, 6.0 m and 10 m. Here the gray shaded portion indicates conditions below the threshold of motion for these grain sizes. Considering Figure 11a first, it is apparent that irrespective of the grain size, τ_{ws} has a potential to transport sediment when A_o exceeds around 1 m. This example sets parameters close to those pertaining for the bulk of the RDS and thus indicates that wave streaming is likely to be implicated in sediment transport under the larger waves and thus might influence ripple formation processes. As the water depth is increased, Figure 11b shows that τ_{ws} decreases and that progressively larger waves are required to mobilize the bed sediments. In the last example, Figure 11c shows that in 10 m water depth τ_{ws} values in all cases fall below the $\tau_{\rm crit}$ values and thus sediment transport would not be expected. While results of the numerical simulations shown in Figure 11 depend heavily on the parameterization used to define δ_w, z_o and $\tau_{\rm crit}$ they provide a guide to the likelihood of bed sediment mobilization by wave streaming not previously considered in this context. They imply that in combination with the flow and turbulence associated with the oscillatory component of the wave-induced flows, large waves have a potential to transport significant amounts of sediment in a thin, high concentration layer in the direction of the wave streaming current. It is considered likely therefore that this mass transport will influence the formation of bed forms in wave-only situations and provide a different mechanism leading to the formation of LWRs. Further it could in principal operate at the same time as those processes forming SWRs.

[34] While here we make assumptions regarding the affects of wave asymmetry we note that the effects of wave asymmetry can reduce greatly (even reverse) the direction of the combined residual (streaming plus asymmetry) in cases where the wave steepness is increased. For the very rough and rippled beds considered here, even weakly asymmetrical waves may produce an offshore mass transport at the edge of the wave boundary layer (wbl) [cf. *Mathisen and Madsen*, 1996] and a pronounced onshore near bed residual jet in the bottom part of the wbl [*Davies and Villaret*, 1999]. Recent numerical modeling based on a solution of the vorticity equation shows also that steady streaming directed along the mild slope of the ripples toward the crest can also be generated at the first order in the wave slope when the sea bed is covered by asymmetric ripples. The steady streaming is found to increase with both the Reynolds number and with the asymmetry index of the ripples. If the streaming currents are competent to mobilize and transport bed sediments they might play a further role in the generation of LWRs through processes not dissimilar to those responsible for current ripples. These effects are likely to enhance rather than suppress the processes outlined above and thus our arguments that residual currents induced by waves may play a role in the formation and maintenance of LWRs are supported further by these considerations.

[35] Turning attention back to the question posed above concerning the superposition of SWRs on LWRs, the evidence suggests that once formed in high wave mobility number conditions, LWRs are persistent bed features. This evidence supports further the suggestion by *Marsh et al.* [1999] that it is rather difficult to change the wavelength of some wave-generated ripples once they have formed. At lower Ψ values, sheet flow ceases and SWRs are again generated over the surface of the LWRs by the familiar vortex shedding mechanisms. Since sediment transport is now reduced and the wave-induced flows probably do not separate above the LWRs, no effective mechanism exists in wave-only flow to remove these features quickly and thus they remain as relict features that coexist with the SWRs for some length of time. Observations in the Delta flume indicate that in these circumstances LWRs are slowly reduced in height by the processes forming new SWRs. These comments are also supported by *Hanes et al.* [2001] who suggest that the geometry of LWRs remains intact long after the hydrodynamic conditions have changed and thus in many field situations are mainly relic features.

[36] Attention is now given to consider why measured wave-generated ripple geometry exhibits such a wide variance in essentially the same hydrodynamic conditions. It is self evident that owing to the time taken for ripples to grow toward equilibrium and for established ripples to respond to changes in the flow, ripple geometry at any given instant will be rarely in equilibrium with the

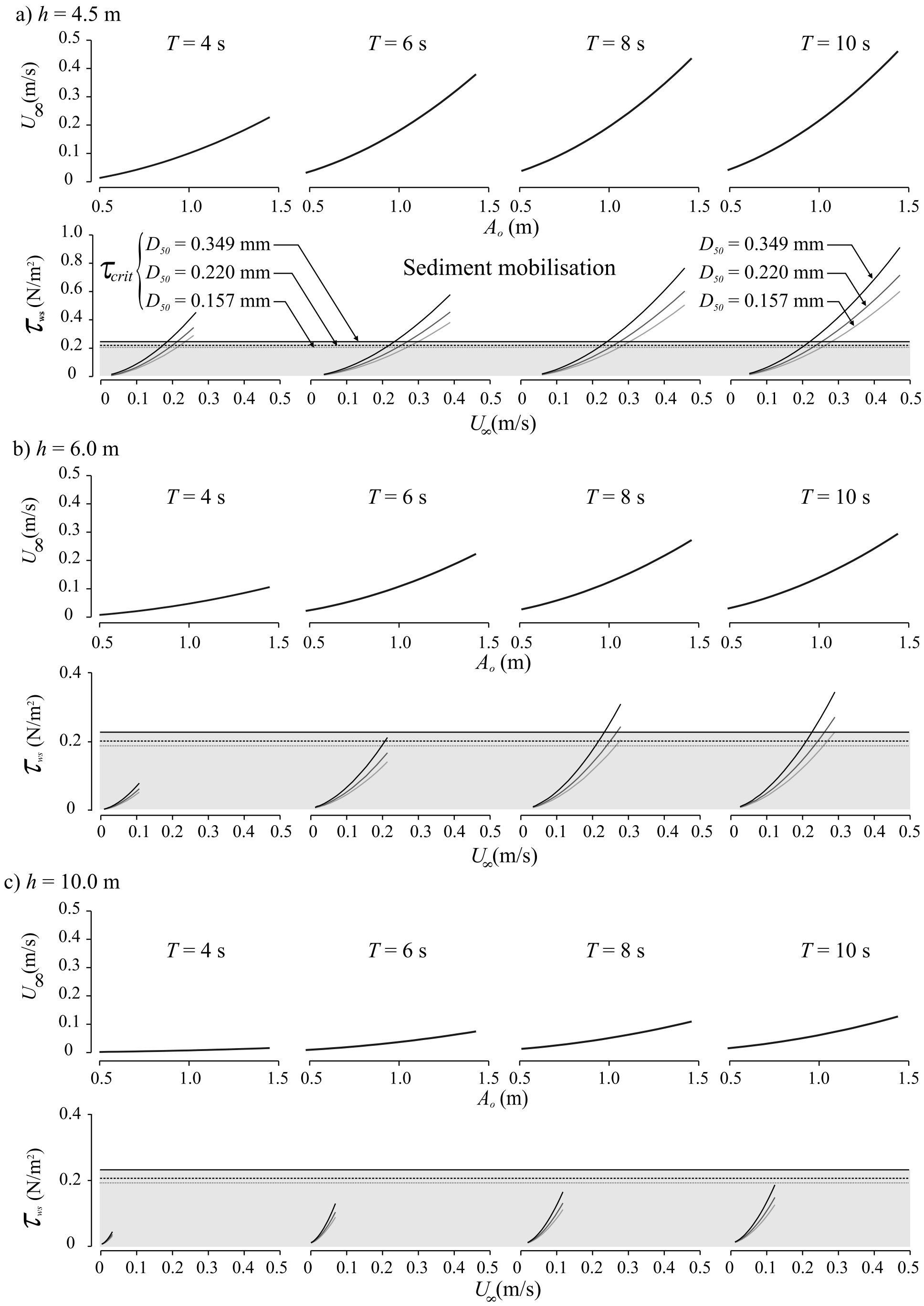

Figure 11. Plots showing potential sediment mobilization and transport by wave streaming for T = 4 s, 6 s, 8 s, and 10s, D_{50} = 0.157 mm, 0.220 mm, and 0.349 mm over the range 0.5 m < A_o < 1.5 m for h = (a) 4.5 m, (b) 6.0 m, and (c) 10.0 m. The top panels of Figures 11a–11c show U_∞ plotted as a function of A_o. The bottom panels of Figures 11a–11c show τ plotted as a function of U_∞.

prevailing flow condition [e.g., *Marsh et al.*, 1999; *Traykovski et al.*, 1999; *Hanes et al.*, 2001]. This disequilibrium is probably further enhanced by complex interactions between SWRs and LWRs identified by *Hanes et al.* [2001]. Thus here we have two possible explanations for the data scatter shown in Figure 10: firstly the highly nonlinear interactions between SWRs and LWRs introduce a further stochastic element into the ripple formation processes and result in the generation of different bed form scales in the same hydrodynamic regime; and secondly, the time taken for the processes of *SWR* formation and the accompanying destruction of LWRs probably depends on factors such as antecedent and present hydrodynamic condition and sediment properties and thus is highly variable. Further factors contributing to data scatter applies particularly to field observations of ripple geometry in a broad and ever changing wave spectrum. In this case there may be no particular dominant near-bed orbital diameter forcing the formation of ripples and their geometry will reflect spatial and temporal variability in the wave field. In these circumstances the idea of a single values for η or λ is meaningless and ripple geometry is best described spectrally. It is likely also that in some cases wave-formed ripples are modified by the presence of a current unrelated to the waves leading directly to data scatter. A further factor to consider is related to the 2-D or 3-D morphology of the ripples. Work reported by *O'Donoghue and Clubb* [2001] suggests that the geometries for 3-D ripples are not related to the local flow in the same way as 2-D ripples. While we do not find any strong evidence for this in the DFD, it is considered likely that some of the variance in measured ripple geometries reported here can be attributed to this factor.

[37] Since prediction of the hydraulic roughness of the bed, k_s, is necessary and often required a priori in many numerical models to predict tidal currents, waves and sediment transport the next question concerns the effects of bed form superposition on k_s. *Grant and Madsen* [1982] show that k_s is a function of the skin friction (related to D_{50}), the form drag (related to ripple geometry) and the near-bed sediment transport. Further, they showed that ripples are responsible for the majority of hydraulic roughness under waves when ripple steepness is >0.1. In terms of their contribution to bed roughness, the relative importance of LWRs can be assessed by considering the total hydraulic roughness k_s defined as

$$k_s = \frac{8\eta^2}{\lambda} + 5\theta_{ws} D_{50} \tag{17}$$

[*Nielsen*, 1992], where $5\theta_{ws}D_{50}$ is the bedload roughness. For the DFD and the SDD the contribution made by bedload roughness to k_s is estimated to be only $O(0.5\%)$ of the bed form roughness and may therefore be neglected for all practical purposes. Taking typical values for LWRs of η = 1 cm and λ = 100 cm, and for SWRs of η = 5 cm and λ = 30 cm, gives k_s values = 0.08 and 1.33, respectively and thus k_s values for SWRs are at least one order of magnitude greater than those for LWRs. Although of lesser importance in terms of bed friction, nevertheless LWRs influence hydrodynamic and associated sedimentary processes and thus require consideration.

[38] Finally, we ask from a practical standpoint which are the best equations to use for predicting the geometry of SWRs and LWRs? A number of widely used empirical expressions have been shown to under perform in cases involving "equilibrium" LWRs. Following established approaches, equations (1)–(4) are shown to have a have a capacity to predict with greater precision η and λ values for the present data set than the published equations defined in Appendix B. However to apply these formulae correctly it is necessary to make a distinction between SWRs and LWRs which is frequently difficult and impracticable. While Figures 3 and 4 indicate it might be possible to do this, there is still considerable uncertainty and thus another approach is desirable. The present data indicate that an alternative might be to use equations (8) and (12) to predict η and ϑ. If the ripple can be classified, equations (9)–(11) can be used to calculate λ or in a simpler approach use $\lambda = \eta/\vartheta$. This method gives estimates of η and λ values that are at least as accurate as existing methods and have the additional advantage that their predictive range spans a wide range of hydrodynamic conditions and ripple morphologies. The use of these expressions in situations not encompassed by existing expressions is therefore recommended.

5. Conclusions

[39] The following points summarize our conclusions.

[40] 1. Acoustic technologies have been applied successfully to measure the height and wavelength of wave-generated bed forms on beds of sandy sediment in the large-scale Delta flume. Given the essential information pertaining to the bed morphology these instruments provide their use in all field and laboratory studies of sediment transport is recommended.

[41] 2. Evidence from flume and field studies shows that SWRs are commonly superimposed upon LWRs.

[42] 3. LWRs observed in the laboratory and in the field were longer and had lower relief than was predicted by models or generally observed previously.

[43] 4. In common with the field data, SWRs observed in the Delta flume were washed out at high wave mobility numbers and LWRs were present most of the time. LWRs were also much more persistent than SWRs are only evolved slowly once established.

[44] 5. Evidence indicates that LWRs are essentially low-relief orbital-like ripples, scaling approximately with A_o, and formed by mechanisms related to the periodic resuspension and deposition of sediment and wave-induced streaming currents.

[45] 6. Nonlinear interactions between SWRs and LWRs and wave spectra are thought to introduce further stochastic processes into ripples generation and are probably implicated in the range of bed form geometry observed in essentially the same hydrodynamic regime.

[46] 7. Time lags between changes in the hydrodynamic conditions and the bed response indicates that the bed history may be as important as the hydrodynamic conditions in determining ripple geometry.

[47] 8. The new predictive equations for wave-generated ripple dimensions span a broad range of sediment and hydrodynamic conditions and negate a need to distinguish between SWRs and LWRs.

[48] 9. These equations may have applications in the interpretation of past depositional environments where robust methods based upon the identification and the interpretation of bed forms preserved in sedimentary facies are needed for accurate environmental reconstruction. This is especially important in cases where LWRs might be misinterpreted as current-generated ripples.

Appendix A: Delta Flume Data (DFD)

[49] Values for the fundamental hydrodynamic and sediment parameters H_s, d_o, ψ, $u_{*\mathrm{ws}}$, η and λ are given in Tables A1 and A2 for the DFD for D_{50} = 0.349 mm and 0.22 mm, respectively. Here we show only those tests where LWRs and SWRs coexisted. The subscripts "s" and "m" refer to SWRs and LWRs, respectively. Table A3 summarizes field data from *Doucette* [2002b] obtained on low-energy beaches with long-period, low-amplitude waves.

Table A1. Suborbital Ripples Coexisting With Megaripples and Associated Hydrodynamics, Delta-2 Tests, With D_{50} = 0.349 mm[a]

Test	H_s, m	d_o, m	Ψ -	U_{*w}, m/s	η_s, m	λ_s, m	η_l, m	λ_l, m
D2-M08	1.4	1.62	127	0.049	0.05	0.60	0.015	2.0
D2-M09	**1.6**	**1.79**	**156**	**0.053**	**0.05**	**0.65**	**0.020**	**2.5**
D2-M10	**1.8**	**1.96**	**186**	**0.057**	**0.05**	**0.64**	**0.020**	**2.0**
D2-M11	1.6	1.76	150	0.053	0.06	0.71	0.020	2.0
D2-M12	1.4	1.62	127	0.049	0.04	0.71	0.016	2.0
D2-M13	1.2	1.39	94	0.044	0.06	0.66	0.008	0.8
D2-M14	1.0	1.18	67	0.039	0.03	0.55	0.004	0.8

[a]Values in bold indicate theoretical sheet flow conditions.

Note that additional data from the Delta flume and data from *Inman* [1957] and *Hume et al.* [1999] used here are summarized by *Williams et al.* [2004].

Appendix B: Definition of Empirical Equations for Prediction of Ripple Geometry

B1. Prediction of Ripple Geometry [*Nielsen*, 1981]

[50] *Nielsen* [1981] computes λ and η values in terms of the skin friction bed shear stress, τ_s, and ψ using separate empirical formulae derived for laboratory and field conditions. For laboratory data, $\eta/\lambda = 0.182 - 0.24\tau_s^{1.5}$; $\lambda/A_o = 2.2 - 0.345\ \psi^{0.34}$; and $\eta/A_o = 0.275 - 0.022\psi^{0.5}$. For field data (where $\psi > 10$), $\eta/\lambda = 0.342 - 0.34\tau_s^{0.25}$; $\lambda/A_o = [(\exp 693 - 0.371 \ln^8 \psi)/(1000 + 0.75 \ln^7 \psi)]$; and $\eta/A_o = 21\psi^{-1.85}$. In these expressions, λ and η = zero at $\psi \geq 156$ when sheet flow conditions apply. *Marsh et al.* [1999] interpret the distinction made here between laboratory and field conditions in terms of the wave spectrum width with laboratory conditions implying monochromatic waves and field conditions implying a broad spread of wave heights and/or periods.

B2. Prediction of Ripple Geometry [*Grant and Madsen*, 1982]

[51] *Grant and Madsen* [1982] relate the geometry of ripples to excess bed shear stress. For orbital ripples this takes the form in the form $\eta/\lambda = 0.16(\tau_s/\tau_c)^{-0.04}$ and $\eta/A_o = 0.22(\tau_s/\tau_c)^{-0.16}$ where $\tau_s/\tau_c < 1.8S_*^{0.6}$, τ_c is the critical bed shear stress for initiation of sediment motion, $S_* = [(\rho_s/\rho) - 1]gD_{50}^{1.5}/4\nu$ and ν is the kinematic viscosity of the fluid. For values of $\tau_s/\tau_c > 1.8S_*^{0.6}$ (i.e., suborbital and anorbital ripples [*Wiberg and Harris*, 1994]), $\eta/\lambda = 0.28S_*^{0.6}(\tau_s/\tau_c)^{-1}$ and $\eta/A_o = 0.48S_*^{0.8}(\tau_s/\tau_c)^{-1.5}$.

Table A2. Suborbital Ripples Coexisting With Megaripples and Associated Hydrodynamics, Delta-2 Tests, With D_{50} = 0.220 mm[a]

Test	H_s, m	d_o, m	Ψ -	U_{*w}, m/s	η_s, m	λ_s, m	η_l, m	λ_l, m
D-2F06	1.0	1.17	104	0.034	0.01	0.55	0.021	1.0
D-2F07	1.2	1.38	147	0.039	0.01	0.48	0.013	1.0
D-2F08	**1.4**	**1.61**	**199**	**0.044**	**0.01**	**0.38**	**0.014**	**1.4**
D-2F09	**1.3**	**1.48**	**169**	**0.041**	**0.01**	**0.43**	**0.012**	**1.3**
D-2F10	1.2	1.39	149	0.039	0.01	0.41	0.013	1.1
D-2F11	1.1	1.28	126	0.037	0.01	0.43	0.015	1.2
D-2F12	1.0	1.17	106	0.035	0.01	0.45	0.015	1.1
D-2F13	0.8	0.95	69	0.032	0.01	0.44	0.019	0.7
D-2F14	0.6	0.73	40	0.024	0.01	0.33	0.020	1.0

[a]Values in bold indicate theoretical sheet flow conditions.

Table A3. Field Data From *Doucette* [2002b, Tables 1 and 2]

h, m	D_{50}, mm	H_s, m	d_o, m	Ψ -	U_{*w}, m/s	η, m	λ, m
0.30	0.58	0.10	0.17	74	0.014	0.03	0.17
0.77	0.35	0.21	1.44	59	0.018	0.09	0.52
0.99	0.35	0.19	1.03	53	0.015	0.09	0.47
0.50	0.51	0.19	0.56	84	0.020	0.06	0.50
0.18	0.40	0.13	1.19	83	0.021	0.06	0.42
0.52	0.40	0.14	0.92	35	0.013	0.05	0.33
0.47	0.62	0.26	2.22	39	0.024	0.11	0.74
0.68	0.62	0.18	0.99	25	0.015	0.14	0.84
0.77	0.62	0.16	0.77	27	0.014	0.11	0.91
0.94	0.62	0.18	0.73	27	0.014	0.11	0.76
1.01	0.62	0.21	0.94	24	0.014	0.10	0.56
1.08	0.62	0.24	1.21	24	0.015	0.07	0.48
0.47	0.62	0.26	2.22	40	0.025	0.09	0.64
0.68	0.62	0.18	0.99	25	0.015	0.10	0.64
0.77	0.62	0.16	0.77	28	0.014	0.12	0.80
0.94	0.62	0.18	0.73	28	0.014	0.13	0.90
1.01	0.62	0.21	0.94	24	0.014	0.11	0.62
1.08	0.62	0.24	1.21	24	0.015	0.07	0.52
0.38	0.38	0.17	0.62	118	0.020	0.05	0.26
0.38	0.38	0.17	0.62	118	0.020	0.05	0.26
0.23	0.43	0.09	1.14	25	0.012	0.05	0.56
0.23	0.43	0.12	1.78	34	0.017	0.03	0.33
0.33	0.41	0.07	0.13	73	0.010	0.02	0.08
0.31	0.53	0.06	0.13	52	0.010	0.02	0.16
0.36	0.53	0.08	0.16	51	0.011	0.03	0.32

B3. Prediction of Ripple Geometry [*Van Rijn*, 1989]

[52] *Van Rijn* [1989] relates η to ψ for irregular waves in the form $\eta/A_o = 0.22$ for $\psi \leq 10$, $\eta/A_o = 2.8 \times 10^{-13}(250 - \psi)^5$ for $10 < \psi < 250$, and $\eta/A_o = 0$ for $\psi > 250$. With knowledge of η, values of λ are then computed using $\eta/\lambda = 0.18$ for $\psi \leq 10$, $\eta/\lambda = 2 \times 10^{-7}(250 - \psi)^{2.5}$ for $10 < \psi < 250$, and $\eta/\lambda = 0$ for $\psi > 250$.

Notation

- A_o orbital amplitude (m);
- D_* dimensionless grain parameter (-);
- D_{50} median grain diameter (mm);
- H wave height (m);
- H_s significant wave height (m);
- L surface gravity wave wavelength (m);
- L_r length scale (m);
- R^2 product moment correlation coefficient (-);
- Re_{grain} grain Reynolds number;
- Re_{wave} orbital Reynolds number;
- S_* dimensionless grain parameter [*Grand and Madsen*, 1982];
- T wave period (s);
- T_p peak wave period (s);
- U_∞ wave streaming velocity (m/s);
- U_{*w} peak wave shear velocity (m/s);
- b Rouse parameter (-);
- d_o wave orbital diameter (m);
- f_w wave friction factor (-);
- g acceleration due to gravity (= 9.81 m/s^2);
- h water depth (m);
- k wave number (-);
- k_s Nikuradse equivalent sand grain roughness ($2.5D_{50}$) (mm);
- s specific gravity of sediment (-);

u_w maximum semiorbital wave speed close to the bed (m/s);
u_{*ws} skin friction (grain roughness) wave-only bed shear velocity (m/s);
w_s grain settling velocity (m/s);
z_o total bed roughness length (m);
ϑ wave ripple steepness (-);
δ_w thickness of the wave boundary layer (m);
γ $\omega^2 h/g$ (-);
η wave ripple height (m);
φ dispersion parameter (-);
κ Karman constant (0.4) (-);
λ wave ripple wavelength (m);
ν kinematic viscosity of the fluid (m^2/s);
θ_{crit} critical Shields parameter (-);
θ_w wave Shields parameter (-)
θ_{ws} wave-only skin friction Shields parameter (-)
ρ fluid density (kg/m^3);
ρ_s sediment density (kg/m^3);
ξ coefficient (-);
τ_s skin friction bed shear stress (N/m^2);
τ_{crit} critical bed shear stress for initiation of sediment motion (N/m^2);
τ_{ws} skin friction (grain roughness) wave-only bed shear stress (N/m^2);
ω radian frequency of waves (rad/s);
ψ mobility number [*Brebner*, 1980] (-).

[53] **Acknowledgments.** The Delta flume experiments were supported by the European Communities through the Access to Research Infrastructure Action of the Improving Human Potential Programme and the UK Natural Environment Research Council (NERC). The paper was completed by JJW during sabbatical leave from NERC in Brazil and the support of Elírio Toldo and Sergio Dillenburg of Instituto de Geociências, Universidade Federal do Rio Grande do Sul (UFRGS) and Lauro Júlio Calliari of Fundação Universidade Federal do Rio Grande (FURG) is gratefully acknowledged. We also acknowledge the helpful comments from Alan G. Davies (University of Bangor, UK), Judith Wolf (POL, UK) and Shunqui Pan (University of Liverpool, UK). We thank the reviewers of this paper for their thorough critiques and helpful suggestions.

References

Amos, C., A. Bowen, D. Huntley, and C. Lewis (1988), Ripple generation under the combined influences of waves and currents on the Canadian continental shelf, *Cont. Shelf Res.*, *8*, 1129–1153.

Andersen, K. H. (1999), The dynamics of ripples beneath surface waves and topics in shell models of turbulence, Ph.D. thesis, Tech. Univ. of Denmark, Copenhagen.

Ardhuin, F., T. G. Drake, and T. H. C. Herbers (2002), Observations of wave-generated vortex ripples on the North Carolina continental shelf, *J. Geophys. Res.*, *107*(C10), 3143, doi:10.1029/2001JC000986.

Bagnold, R. A. (1946), Motion of waves in shallow water – interaction between waves and sand bottoms, *Proc. R. Soc. London, Ser. A*, *187*, 1–15.

Bell, P. S., and P. D. Thorne (1997), Application of a high resolution acoustic scanning system for imaging sea bed microtopography, paper presented at 7th International Conference on Electronic Engineering in Oceanography, Inst. of Electr. Eng., Southampton, UK, 23–25 June.

Bell, P. S., P. D. Thorne, and J. J. Willilams (1998), Acoustic measurements of sand ripple profile evolution under controlled wave conditions, paper presented at 4th European Conference on Underwater Acoustics, Eur. Comm., Rome, 21–25 Sept.

Boyd, R., D. L. Forbes, and D. E. Heffler (1988), Time-sequence observations of wave-formed sand ripples on an ocean shore face, *Sedimentology*, *35*, 449–464.

Brebner, A. (1980), Sand bed-form lengths under oscillatory flow, paper presented at 17th International Conference on Coastal Engineering, Am. Soc. of Civ. Eng., New York, N. Y.

Carstens, M. R., R. M. Nielson, and H. D. Altinbilek (1969), Bedforms generated in the laboratory under oscillatory flow: Analytical and experimental study, *Tech. Mem. 28*, U.S. Corps of Eng., Coastal Eng. Res. Cent., Fort Belvoir, Va.

Crawford, A. M., and A. E. Hay (2001), Linear transition ripple migration and wave orbital velocity skewness: Observations, *J. Geophys. Res.*, *106*, 14,113–14,128.

Davies, A. G., and C. Villaret (1999), Eulerian drift induced by progressive waves above rippled and very rough beds, *J. Geophys. Res.*, *104*, 1465–1488.

Dingler, J. R. (1974), Wave-formed ripples in nearshore sands, Ph.D. thesis, 136 pp., Univ. of Calif., San Diego.

Dingler, J. R., and D. L. Inman (1976), Wave-formed ripples in near-shore sands, paper presented at 15th Conference of Coastal Eng., Am. Soc. of Civ. Eng., Honolulu, Hawaii, USA.

Doucette, J. S. (2002a), Bedform migration and sediment dynamics in the nearshore of a low-energy sandy beach in southwestern Australia, *J. Coastal Res.*, *18*(3), 576–591.

Doucette, J. S. (2002b), Ripple grain size sorting and geometry prediction on low-energy sandy beaches, *Sedimentology*, *49*, 483–503.

Drake, D. E., and D. A. Cacchione (1989), Field observations of bed shear stress and sediment resuspension on continental shelves, Alaska and California, *Cont. Shelf Res.*, *6*, 415–429.

Faraci, C., and E. Foti (2002), Geometry, migration and evolution of small-scale bedforms generated by regular and irregular waves, *Coastal Eng.*, *47*, 35–52.

Fredsøe, J. (1984), Turbulent boundary layer in wave-current motion, *J. Hydraul. Eng.*, *110*, 1103–1120.

Gallagher, E. L., S. Elgar, and E. B. Thornton (1998), Megaripple migration in a natural surf zone, *Nature*, *394*, 165–168.

Grant, W. D., and O. S. Madsen (1982), Movable bed roughness in unsteady oscillatory flow, *J. Geophys. Res.*, *87*, 469–481.

Hanes, D. M., V. Alymov, Y. S. Chang, and C. Jette (2001), Wave-formed sand ripples at Duck, North Carolina, *J. Geophys. Res.*, *106*, 22,575–22,592.

Hay, A. E., and D. J. Wilson (1994), Rotary sidescan images of nearshore bedform evolution during a storm, *Mar. Geol.*, *119*, 57–65.

Hume, T. M., M. O. Green, and J. W. Oldman (1999), What happens at the seabed off a headland during a tropical cyclone, in *Coastal Sediments '99*, pp. 1836–1851.

Inman, D. L. (1957), Wave-generated ripples in nearshore sands, *Tech. Mem. 100*, 66 pp. U.S. Army Corps of Eng., Washington, D. C.

Jette, C. D. (1997), Wave-generated bedforms in the near-shore sand environment, Ph.D. dissertation, Univ. of Fla., Gainesville.

Jette, C. D., and D. M. Hanes (1998), High-resolution sea-bed imaging: An acoustic multiple transducer array, *Meas. Sci. Technol.*, *8*, 787–792.

Khelifa, A., and Y. Ouellet (2000), Prediction of sand ripple geometry under waves and currents, *J. Waterw. Port Coastal Ocean Eng.*, *126*(1), 14–22.

Kos'yan, R. D. (1988), Study of sand microforms in the nearshore zone, *Mar. Geol.*, *83*, 63–78.

Li, M. Z., and C. L. Amos (1999), Sheet flow and large wave ripples under combined waves and currents: Field observations, model predictions, and effects on boundary layer dynamics, *Cont. Shelf Res.*, *19*, 637–663.

Li, M. Z., L. D. Wright, and C. L. Amos (1996), Predicting ripple roughness and sand resuspension under combined flows in a shoreface environment, *Mar. Geol.*, *130*, 139–161.

Lofquist, K. E. B. (1978), Sand ripple growth in an oscillatory-flow water tunnel, *Tech. Pap. 78-5*, U.S. Army Coastal Eng. Res. Cent., Vicksburg, Miss.

Longuet-Higgins, M. S. (1953), Mass transport in water waves, *Philos. Trans. R. Soc. London, Ser. A*, *345*, 535–581.

Marsh, S. W., C. E. Vincent, and P. D. Osborne (1999), Bedforms in a laboratory wave flume: An evaluation of predictive models for bedform wavelengths, *J. Coastal Res.*, *15*(3), 624–634.

Mathisen, P. P., and O. S. Madsen (1996), Waves and currents over a rippled bed: 1. Bottom roughness experienced by waves in the presence and absence of a current, *J. Geophys. Res.*, *101*, 16,533–16,542.

Metje, N., J. J. Williams, and L. E. Coates (2001), Quantification of bed morphology and sediment transport beneath a large field deployment frame, *Coastal Eng.*, *3*, 2672–2681.

Miller, M. C., and P. D. Komar (1980), A field investigation of the relationship between oscillation ripple spacing and the near-bottom water orbital motions, *J. Sediment. Petrol.*, *50*(1), 0183–0191.

Mogridge, G. R., and J. W. Kamphius (1972), Experiment on bed form generation by wave action, paper presented at 13th Coastal Engineering Conference, Am. Soc. of Civ. Eng., Vancouver, Can.

Mogridge, G. R., M. H. Davies, and D. H. Willis (1994), Geometry prediction for wave-generated bedforms, *Coastal Eng.*, *22*, 255–286.

Nielsen, P. (1981), Dynamics and geometry of wave-generated ripples, *J. Geophys. Res.*, *86*, 6467–6472.

Nielsen, P. (1992), *Coastal Bottom Boundary Layers and Sediment Transport*, World Sci., Hackensack, N. J.
O'Connor, B. A., H. S. Kim, and J. J. Williams (1994), Hydrodynamics of random wave boundary-layers, paper presented at Coastal Dynamics '94, Am. Soc. of Civ. Eng., Univ. Politèc. de Catalunya, Barcelona, Spain, 21–25 Feb.
O'Donoghue, T., and G. S. Clubb (2001), Sand ripples generated by regular oscillatory flow, *Coastal Eng.*, *44*, 101–115.
Osborne, P. D., and C. E. Vincent (1993), Dynamics of large and small scale bedforms on a macrotidal shoreface under shoaling and breaking waves, *Mar. Geol.*, *115*, 207–226.
Ribberink, J. S., and A. A. Al-Salem (1994), Sediment transport in oscillatory boundary layers in cases of rippled beds and sheet flow, *J. Geophys. Res.*, *99*, 12,707–12,727.
Sato, S., and K. Horikawa (1986), Laboratory study on sand transport over ripples due to asymmetric oscillatory flows, paper presented at 20th International Coastal Engineering Conference, Am. Soc. of Civ. Eng., Taipei, Taiwan.
Soulsby, R. L. (1997), *Dynamics of Marine Sands: A Manual for Practical Applications*, 249 pp., Thomas Telford, London.
Southard, J. B., J. M. Lambie, D. C. Frederico, H. T. Pile, and C. R. Wiedman (1990), Experiments on bed configurations in fine sands under bidirectional purely oscillatory flow, and the origin of hummocky cross-stratification, *J. Sediment. Petrol.*, *60*, 1–17.
Thornton, E. B., J. L. Swayne, and J. R. Dingler (1998), Small-scale morphology across the surf zone, *Mar. Geol.*, *145*, 173–196.
Tjerry, S. (1995), Morphological calculation of dunes in alluvial rivers, Ph.D. thesis, Tech. Univ. of Denmark, Copenhagen.
Torrence, C., and G. P. Compo (1998), A practical guide to wavelet analysis, *Bull. Am. Meteorol Soc.*, *79*, 61–78.
Traykovski, P., A. E. Hay, J. D. Irish, and J. F. Lynch (1999), Geometry, migration, and evolution of wave orbital ripples at LEO-15, *J. Geophys. Res.*, *104*, 1505–1524.
Van Rijn, L. C. (1989), *Handbook of Sediment Transport by Currents and Waves*, Delft Hydraulics, Delft, Netherlands.
Vincent, C. E., S. W. Marsh, M. P. Webb, and P. D. Osborne (1999), Spatial and temporal structures of suspension and transport over megaripples on the shore face, *J. Geophys. Res.*, *104*, 11,215–11,224.
Vincent, C. E., D. M. Hanes, C. M. Dohmen-Janssen, G. Klopman, M. Mclean, C. Obhrai, and J. S. Ribberink (2001), Suspension by regular and groupy waves over bedforms in a large wave flume (SISTEX99), in *Coastal Dynamics'01*, pp. 303–312, Am. Soc. of Civ. Eng., Reston, Va.
Vongvisessomjai, S. (1984), Oscillatory ripple geometry, *J. Hydraul. Eng.*, *110*(3), 247–266.
Wiberg, P. L., and C. K. Harris (1994), Ripple geometry in wave dominated environments, *J. Geophys. Res.*, *99*, 775–789.
Wikramanayake, P. N. (1993), Velocity profiles and suspended sediment transport in wave-current flows, Ph.D. thesis, 285 pp., Mass. Inst. of Technol., Cambridge.
Williams, J. J., P. S. Bell, P. D. Thorne, K. Trouw, P. J. Hardcastle, and J. D. Humphery (2000), Observed and predicted vertical suspended sediment concentration profiles and bedforms in oscillatory-only flow, *J. Coastal Res.*, *16*(3), 698–708.
Williams, J. J., P. S. Bell, L. E. Coates, N. Metje, and R. Selwyn (2003), Laboratory study of interactions between a large instrument deployment frame and oscillatory flow on a sandy bed, *Cont. Shelf Res.*, *23*, 355–375.
Williams, J. J., P. S. Bell, P. D. Thorne, N. Metje, and L. E. Coates (2004), Measurement and prediction of wave-generated suborbital ripples, *J. Geophys. Res.*, *109*, C02004, doi:10.1029/2003JC001882.

P. S. Bell, P. D. Thorne, and J. J. Williams, Proudman Oceanographic Laboratory, Joseph Proudman Building, 6, Brownlow Street, Liverpool L3 5DA, UK. (jjw@pol.ac.uk)